BIODEGRADABLE POLYESTER MICROPARTICLES: SUSTAINABLE PRODUCTION, ANALYSIS OF DEGRADATION, AND NOVEL APPLICATIONS

A Dissertation

Presented to the Faculty of the Graduate School

of Cornell University

In Partial Fulfillment of the Requirements for the Degree of

Doctor of Philosophy

by

Hooman Torabi

August 2023

BIODEGRADABLE POLYESTER MICROPARTICLES: SUSTAINABLE PRODUCTION, ANALYSIS OF DEGRADATION, AND NOVEL APPLICATIONS

Hooman Torabi, Ph. D.

Cornell University 2023

Polyesters are a family of both synthetic and natural polymers extensively used in a wide variety of applications from commodity materials to advanced engineering parts of space crafts. Polyester microparticles are produced intentionally for specific applications in agriculture, cosmetics, hygiene products, and medicine businesses. These particles could also be generated from mechanical or microbial degradation of larger parts and find their way inside the marine food chain, endangering the ecosystem as well as national and international food safety.

To address such issues, we targeted bioproduction of polyhydroxy alkanoates (PHA) as they are non-toxic and fully biodegradable. Microbial production of such materials is limited due to the high cost of production, mostly from the carbon source. In this regard, we investigated the possibility of using manure as a sustainable feed stock addressing the environmental and economic concerns associated with manure management.

Standard biodegradation assessment tests, generally known as soil burial methods, are extremely time-taking and their results are hard to reproduce. Thus, we devised and fabricated a microfluidic platform to immobilize polymeric microparticles and analyze their enzymatic degradation, in a close-to-static microflow condition, mimicking natural microbial degradation. We further developed a mathematical model to find the kinetic parameters of this

class of degradation assuming shrinking particle- shrinking core model of transport phenomena.

Polyhydroxy butyrate (PHB), the simplest form of PHA, is generally accepted as a hard-to-process thermoplastic due to its high degree of crystallinity, limiting its wide-spread application. We sought to take advantage of and even enhance this property as it can affect the biodegradation rate, making it a great platform for a controlled release system of micronutrients to plants and crops. Optimizing the genetic modification, genotype used, and culture conditions, we were able to bio-produce high-molecular weight PHB with 65% crystallinity. Loading this PHB with 30% of iron nanoparticles (micronutrient) resulted in a nanocomposite with 30% crystallinity which later was found to be an effective nano fertilizer for delivery of cargo to the soil within 10 weeks of addition to the soil. Pot experiments demonstrated that plants growing on soil amended with this nano fertilizer grew faster than control groups.

BIOGRAPHICAL SKETCH

Hooman Torabi was born on September 5th,1989, in Mashhad, Iran. He obtained his B.Sc. degree in Chemical Engineering from Quchan University of Technology, Quchan, Iran in 2012. He further completed his M.Sc. study in Chemical Engineering with a focus on Polymer Engineering from Sharif University of Technology, Tehran, Iran in early 2015. Afterwards, he pursued his studies on Polymer Chemistry at Florida International University, Miami, FL, obtaining his second M.Sc. degree in Chemistry. He joined Cornell University in summer 2020 to pursue his Ph.D. degree. During his Ph.D. studies, he worked under the supervision of Dr. Alireza Abbaspourrad, focusing on biodegradable polyesters. Hooman's research interest is primarily focused on sustainable and microbial production, analysis of degradation, and novel applications of biodegradable polyesters. Upon completing his Ph.D. studies at Cornell University, Hooman plans to pursue his career in industry as a research and development scientist to enhance the use of green materials for a wide variety of everyday applications. His time at Cornell University has prepared him to apply his knowledge and expertise to his future career goals.

To My Beloved Family

ACKNOWLEDGMENTS

I would like to express my gratitude to everyone who has supported me throughout my academic journey and the completion of this dissertation. First and foremost, I would like to thank my advisor, Dr. Alireza Abbaspourrad, for his guidance, support, and mentorship throughout my Ph.D. studies. His passion for research, his commitment to teaching, and his dedication to his students have been an inspiration to me. I would also like to thank my committee members, Dr. Terry E. Acree and Dr. Sijin Li, for their valuable feedback and insightful comments that helped shape and improve this dissertation.

I would like to express my sincere gratitude to our industry collaborators at BASF North America and New York Pollution Prevention Institute for their generous support in funding this research project.

I extend my gratitude to my colleagues in the Abbaspourrad Lab for their unwavering support, collaboration, and friendship throughout my Ph.D. journey. I would also like to express my appreciation to the staff at Cornell University for providing me with valuable resources.

More importantly, I would like to extend my heartfelt thanks to my family, for their unwavering love, support, and encouragement throughout my life and academic journey. Their sacrifices and hard work have made it possible for me to pursue my dreams and achieve my goals. I am forever grateful for their unconditional love.

TABLE OF CONTENTS

LIST OF FIGURES

LIST OF TABLES

Introduction

Over the past 50 years, petroleum-based plastics have become an essential commodity of modern life with the annual production rate of over 380 million tons (as of 2015).[1] A major portion of these materials, which are discarded into the environment, impact land and marine ecosystems due to their nonbiodegradability. In this regard, a global effort has been devoted to minimizing the use of nondegradable plastics, and ecofriendly alternatives are in high demand by consumers, industry, and regulators. Several biopolymers, such as polycaprolactone (PCL), polylactic acid (PLA), and polyhydroxy alkanoates (PHAs) have been extensively studied for a wide range of applications. Polyhydroxy alkanoates (PHAs), are a family of biodegradable polyesters first discovered by Maurice Lemoigne produced by different microorganisms which exhibit many of the same mechanical, physical, and chemical characteristics of everyday plastics. PHAs are considered favorable materials for biomedical and biotechnological applications,[2] and are suitable candidates to replace petroleum-based plastics for packaging purposes.[3] However, widespread applications of PHAs are currently limited due to the high production costs associated with microbial production. It has been reported that over 50% of the production costs of microbially produced bioplastics are related to the feedstock, or carbon source.[4] As a result, numerous studies have been focused on PHA production using cost-effective and sustainable carbon sources especially, from the food industry and agricultural wastes.[5] Aliphatic and aliphatic-aromatic polyesters, including PHAs, are considered fully compostable polymers and their microbial degradation has been previously studied. [6, 7] Although field test methods such as soil burial and composting simulate environmental degradation conditions, they are time-consuming and have a limited scope of analysis. For instance, soil burial biodegradation and

composting tests is validated after 180 days and 24 months according to ISO 17088 and ASTM D5988, respectively. [8] In this regard, there is a growing demand for a fast and reliable technique for performing and mathematically modelling enzymatic degradation. This technique needs to be standardized to yield comparable results from one study to another. Development of a new standard technique facilitates evaluation of the degradability of developing products, identifying and engineering new enzymes, and optimization of conditions for degradation of plastics. Food demand is projected to increase by 70% for the world population by 2050. To meet this demand, new technologies need to be developed to lead to a more sustainable and efficient agriculture industry. Accumulation of chemicals in soil rising from extensive use of fertilizers has become a major concern globally. Moreover, common fertilizers are unable to effectively provide micronutrients to crops leading to a decrease in soil and product quality. [9] In this regard, an environmentally friendly substitution needs to be introduced to address the abovementioned issues. Incorporation of nanotechnology and agriculture industry can be a promising approach for not only addressing environmental concerns, but also guarantee food security in the upcoming decades.

References

(1) Geyer, R.; Jambeck, J. R.; Law, K. L. Production, Use, and Fate of All Plastics Ever Made. *Science advances* **2017**, *3* (7), e1700782.

(2) Kalia, V. C.; Ray, S.; Patel, S. K.; Singh, M.; Singh, G. P. The Dawn of Novel Biotechnological Applications of Polyhydroxyalkanoates. In *Biotechnological applications of polyhydroxyalkanoates*; Springer, 2019; pp 1–11.

(3) Bugnicourt, E.; Cinelli, P.; Lazzeri, A.; Alvarez, V. A. Polyhydroxyalkanoate (PHA): Review of Synthesis, Characteristics, Processing and Potential Applications in Packaging. **2014**.

(4) Kumar, M.; Rathour, R.; Singh, R.; Sun, Y.; Pandey, A.; Gnansounou, E.; Lin, K.-Y. A.; Tsang, D. C.; Thakur, I. S. Bacterial Polyhydroxyalkanoates: Opportunities, Challenges, and Prospects. *Journal of Cleaner Production* **2020**, *263*, 121500.

(5) Favaro, L.; Basaglia, M.; Casella, S. Improving Polyhydroxyalkanoate Production from Inexpensive Carbon Sources by Genetic Approaches: A Review. *Biofuels, Bioproducts and Biorefining* **2019**, *13* (1), 208–227.

(6) Herzog, K.; Müller, R.-J.; Deckwer, W.-D. Mechanism and Kinetics of the Enzymatic Hydrolysis of Polyester Nanoparticles by Lipases. *Polymer degradation and stability* **2006**, *91* (10), 2486–2498.

(7) Scandola, M.; Focarete, M. L.; Frisoni, G. Simple Kinetic Model for the Heterogeneous Enzymatic Hydrolysis of Natural Poly (3-Hydroxybutyrate). *Macromolecules* **1998**, *31* (12), 3846–3851.

(8) Breulmann, M.; Künkel, A.; Philipp, S.; Reimer, V.; Siegenthaler, K. O.; Skupin, G.; Yamamoto, M. Polymers, Biodegradable. *Ullmann's encyclopedia of industrial chemistry* **2000**.

(9) Guha, T.; Gopal, G.; Kundu, R.; Mukherjee, A. Nanocomposites for Delivering Agrochemicals: A Comprehensive Review. *Journal of Agricultural and Food Chemistry* **2020**, *68* (12), 3691–3702.

Chapter 1: Sustainable Production

Xylose-rich Horse Manure Hydrolysate as the Sole Carbon Source for Bacterial Production of Polyhydroxy Butyrate (PHB) Using Engineered *E. coli*

ABSTRACT

We investigated the possibility of using horse manure hydrolysates (HMH) as the sole carbon source for bacterial production of Polyhydroxy Butyrate (PHB) by engineered *E. coli*. HMH was prepared by acid hydrolysis of horse manure. Over 90% of toxic furan byproducts were removed to yield detoxified HMH (D-HMH). Chemical analysis of hydrolysates revealed the presence of xylose and arabinose at high concentrations. *E. coli* BL21 strain was genetically engineered to produce PHB when D-HMH or xylose (control) were used as the sole carbon feedstock. Cells were incubated for both 48 h and 72 h followed by PHB extraction. The molecular weight measurements and thermal characterization of the PHB produced were similar whether the cells were fed D-HMH or xylose. Our results led to a facile method for valorization of manure by introducing its hydrolysates as a sustainable feed stock for bacterial production of PHB.

Keywords: Horse manure, Manure hydrolysates, Xylose, Sustainable, Polyhydroxy Butyrate, Waste-to-Value, *E. coli*

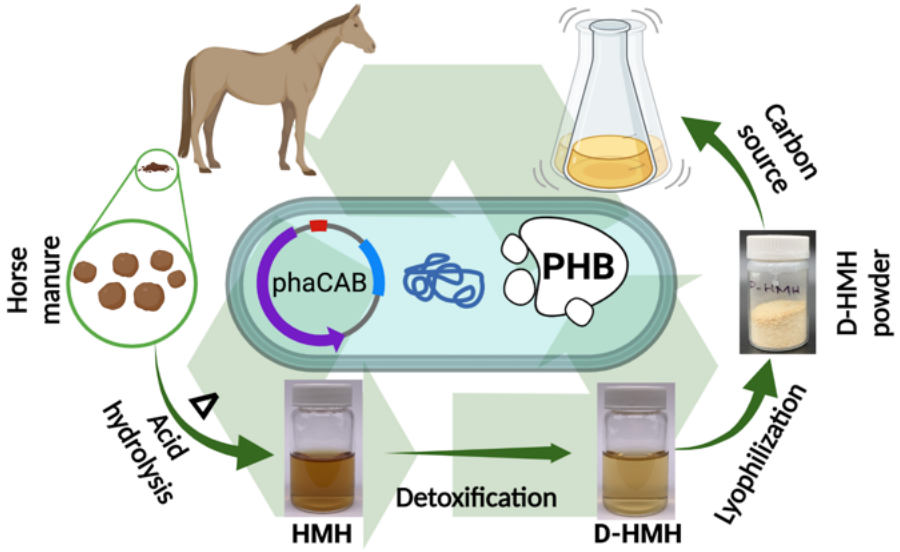

Figure 1. 1: Graphical abstract

INTRODUCTION

Over the past 50 years, petroleum-based plastics have become an essential commodity of modern life with the annual production rate of over 380 million tons (as of 2015).[1] A major portion of these materials, which are discarded into the environment, are impacting land and marine ecosystems due to their non-biodegradability. In this regard, a global effort has been devoted to minimizing the use of non-degradable plastics and eco-friendly alternatives are in high demand by consumers, industry, and regulators. Several biopolymers, such as polycaprolactone (PCL), polylactic acid (PLA), and polyhydroxy alkanoates (PHA)s have been extensively studied for a wide range of applications.

PHAs are a family of biodegradable polyesters produced by different microorganisms which exhibit many of the same mechanical, physical, and chemical characteristics of everyday plastics. PHAs are considered favorable materials for biomedical and biotechnological [2] applications and are suitable candidates to replace petroleum-based plastics for packaging purposes.[3]

Biological pathways in natural PHA-producing microorganisms leading to biosynthesis, storing/ secretion of PHAs, and the strain developments have been previously discussed in detail.[4] Despite the absence of genes required for PHA biosynthesis, *E. coli* has been introduced as a superior platform for bioplastic production because its ease of genetic modification, absence of depolymerization genes,[5] and high intracellular PHA accumulation up to 90% of its cell dry weight.[6]

Widespread applications of PHAs are currently limited due to the high production costs associated with microbial production. To address this issue, up-scaling challenges have been

reviewed[7], bioreactor scale production has been previously discussed,[8] and sustainable approaches to downstream processing has been explored.[9] It has been reported that over 50% of the production costs of microbially produced bioplastics are related to the feedstock, or carbon source.[10] As a result, numerous studies have been focused on PHA production using cost-effective and sustainable carbon sources especially, from the food industry and agricultural wastes.[6]

Manure is usually considered waste, and proper manure management is crucial for the horse, dairy, and poultry industries to minimize associated pollution. As a result, several waste-to-value approaches for more efficient and economical manure management systems have been reported. Several studies reported using manure biomass for biofuel production owing to its high cellulose and hemicellulose content.[11] Manure has also recently been used as a substance of interest for sustainable PHA production by *C. necator* using mixtures of vegetable oil waste and digested chicken manure.[12] Carbon dioxide and poultry wastes were used as carbon sources by *Nostoc muscorum Agardh*, to produce 750 mg of PHA per liter of culture media.[13] The potential of different mixed microbial consortia for PHA production using poultry and dairy manure has also been investigated.[14–16] This study serves as a proof of concept of a waste-to-value approach toward the bacterial synthesis of Polyhydroxy Butyrate (PHB) by engineered *E. coli* using horse manure hydrolysates as the sole carbon source; this has not been reported to date.

EXPERIMENTAL SECTION

Preparation and Detoxification of Horse Manure Hydrolysates

Manure hydrolysates were prepared according to a previously reported method[17] with some modifications. In summary, horse manure, provided by Placid Hill Farms (Troy, NY), was dried

at 85°C for 48 h. It was then chopped, powdered, and passed through a 2 mm sieve. This powder was then transferred into autoclave bottles containing 6% sulfuric acid at a total solid-to-liquid (S:L) ratio of 0.1. This mixture was autoclaved for 1 h at 120°C. The dark brown liquor was then filtered and neutralized via the following overliming method. Calcium hydroxide powder was slowly added to the mother liquor while stirring to bring the pH to 10 then after 3mins, the pH was reduced to neutral condition by addition of dilute sulfuric acid. Insoluble salts were removed by filtration to yield a light brown horse manure hydrolysate (HMH) solution. To remove toxic furan byproducts, 15 g of activated charcoal was added to 1 L of HMH and stirred at 35°C for 3.5 h.[18] Activated charcoal was removed from the yellow solution of detoxified horse manure hydrolysate (D-HMH). Finally, the D-HMH solution was lyophilized to yield an off-white D-HMH powder for bacterial production of PHB. Aliquots of hydrolysates were collected prior to lyophilization for chemical composition analysis.

Culture Conditions and PHB Production

A single colony of Recombinant *E. coli* strain from an LB agar plate was inoculated into 5 ml of LB medium containing 100 µg/mL ampicillin. The culture was incubated for 18 h at 37°C with 250 rpm reciprocal shaking. To study the growth kinetics of the cells in presence of D-HMH, 0.3 mL of seeded cells was added to 25 mL flasks containing 10 mL of LB and D-HMH at concentrations of 1, 2, and 3% (w/v). For PHA production, 1 mL of cultured cells were added to a 250 mL baffled flask containing 100 mL of LB media and 100 µg/mL ampicillin sodium followed by incubation at 37°C. When the optical density of the culture reached 0.6-0.8 (approximately 3 h), isopropyl-β- D-thiogalactoside (IPTG) was added for a final concentration of 100 mg/L. After 1 h, D-HMH or xylose was added with the final sugar concentration of 2% (w/v). The cells were then incubated for designated time frames.

PHA Extraction and Purification

Cells were harvested by centrifugation at 4000xg for 30 min at 4°C, lyophilized and weighed. Dry cell mass was transferred to 15 mL pressure tubes with Teflon stoppers containing 12 mL of chloroform, stirred at 100°C for 4 h to extract intracellular PHA. Cell debris were then removed, and the PHB-containing supernatant was concentrated and further purified by precipitation in ice-cold methanol.

Analytical Methods

The chemical composition of the horse manure hydrolysates was assessed using a high-performance liquid chromatography (HPLC, Agilent 1100) machine equipped with an Aminex HPX-87H column (Bio-Rad, USA). Sulfuric acid (0.01N) was used as the mobile phase at a flow rate of 0.2 mL/min at 40°C. UV-vis spectroscopy was performed to analyze the hydrolysates using a Shimadzu UV2600 spectrophotometer. The optical density of culture media was measured by SpectraMax iD3 plate reader. Number average molecular weight (Mn) and weight average molecular weight (Mw) of the produced PHBs was measured by gel permeation chromatography (GPC) analysis, calibrated using polystyrene standards and THF as the mobile phase. The FT-IR spectrum of PHB was recorded using IRAffinity-1S (Shimadzu, Japan) equipped with an ATR module. ^{1}H-NMR spectrum was recorded using Bruker 500MHz with $CDCl_3$ as the solvent and enhanced relaxation delay. Differential Scanning Calorimetry (DSC) tests were performed using Q2000 TA Instruments (New Castle, DE, USA) according to ASTM D3418 to measure melting temperature (T_m), glass transition temperature (T_g), Degradation temperature (Td), melting enthalpy (ΔH_m), and crystallinity (X_c). Statistical analysis was performed using OriginPro 9.0. OriginLab Corp., Northampton, MA.

RESULTS AND DISCUSSIONS

Sugar Yield and Chemical Composition of Horse Manure Hydrolysates

About 50% of horse manure is reportedly composed of water-insoluble cellulose and hemicellulose.[19] To generate water-soluble sugars, horse manure was acid hydrolyzed and treated with activated charcoal to remove toxic compounds. Total furan content (TFC) was measured by UV-vis spectroscopy (**Fig 1.2**) before and after detoxification. Considering that the furans' extinction coefficient is equal to 0.127 mg/L at 278nm,[20] the TFC was found to be 100.4 mg/L and 8.8 mg/L for HMH and D-HMH, respectively.

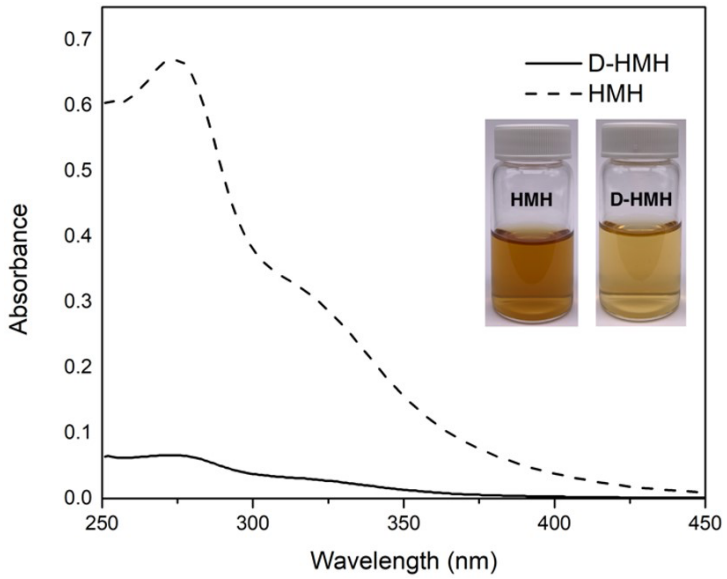

Figure 1. 2: UV-vis spectrum of hydrolysates (20x diluted in water). λ_{max}: 278 nm.

Table 1.1 summarizes the composition of hydrolysate before and after detoxification. As shown, the active charcoal treatment successfully removed 90% of the furans, a marked improvement over a previously reported attempt [21] in which, only 50% of the furan was removed. These findings were also confirmed by HPLC analysis for furfural content measurements (**Table 1.1**).

The HPLC analysis demonstrates that the sugar composition of hydrolysates is mostly composed of xylose (over 78%). Arabinose and glucose contents were also quantified (**Table 1.1**). Total amount of solids was 2.1% w/v for D-HMH. In addition to this, detoxification slightly changed the sugar concentration by removal of approximately 5% of xylose and 20% of glucose. Overall, our method resulted in removal of approximately 4% of total sugar, which is far less than previously reports [18, 21] in which, ion exchange resins were used for detoxification. Detoxification did not significantly remove acetic acid, which is consistent with previous research.[18] Previous studies reported the necessity of acetate removal at concentrations greater than 2%,[21, 22] which is ~10 times more than what we found in D-HMH. As a result, such low acetate concentration does not affect the cell growth rates, which is supported by other reports.[17, 23] Formic acid and HMF were not detected in the hydrolysates. Moreover, levulinic acid, which when present, can alter bioproduced PHA composition,[23] was not detected in hydrolysates.

Table 1. 1: Chemical Composition of Horse Manure Hydrolysate

Carbon source	Sugar (g/L)	Sugar composition (%)			Acetic acid (%)	Furfural (mg/L)	HMF (mg/L) [a]	L. A [b] (mg/L) [a]	F. A [c] (mg/L) [a]
		Xylose	Arabinose	Glucose					
HMH	18.27	78.5	17.5	4.0	0.220	77.3	ND	ND	ND
D-HMH	17.54	78.4	18.1	3.4	0.215	7.2	ND	ND	ND

[a] Detection limit was 1 mg/L. [b] Levulinic acid. [c] Formic acid

PHB Synthesis with Manure Hydrolysate

In order to study the possible growth-inhibitory effects posed by D-HMH on *E. coli*, we indirectly monitored the growth kinetics of the cells in presence of 1%, 2%, and 3% (w/v) of D-HMH in LB media by measuring the optical density at 550 nm (OD_{550}) every 30 min for 7 h and compared them to that of the control (0% D-HMH). Our findings showed that up to 2% of D-

HMH in culture media does not significantly change the growth rates. Upon addition of 3% D-HMH, cells show slower growth kinetics, even though the optical density reaches to 0.6 after 7 hours of incubation (**Fig 1. 3**). Overall, it could be concluded that acetate ions and other impurities, presented in D-HMH, did not show growth inhibition to *E. coli* with up to 3% (w/v) of D-HMH.

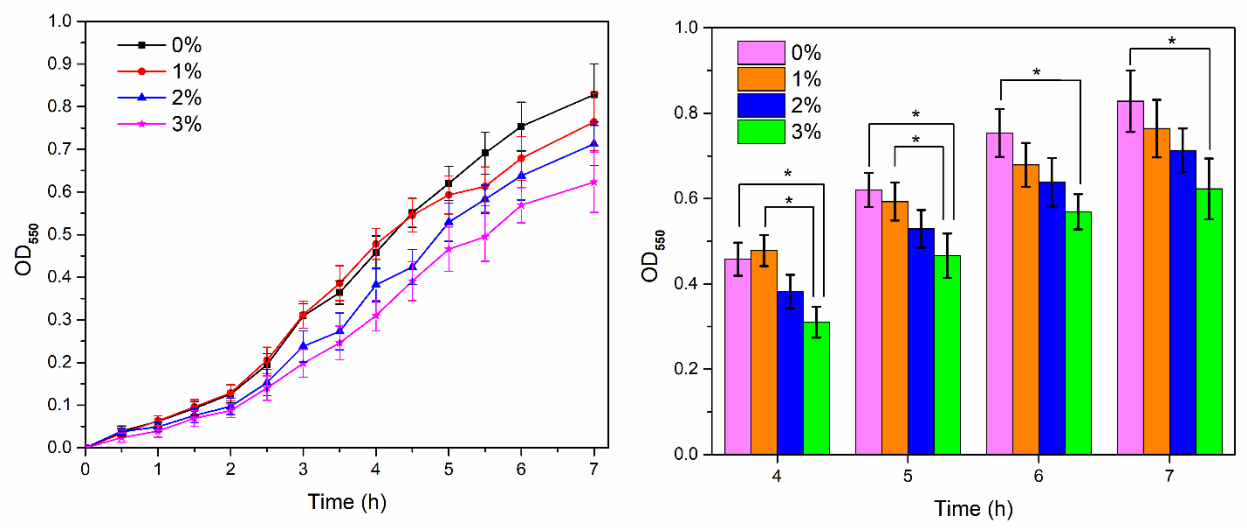

Figure 1. 3: (left) Growth rate of engineered E. coli in presence of D-HMH. (right) statistical analysis of growth rates by one-way ANOVA Tukey's test. Error bars represent the standard deviation of the mean with 95% confidence interval Statistical significance of data (*$p < 0.05$)

D-HMH was used as the sole carbon source for PHB production using engineered *E. coli* which were incubated after addition for two-time intervals, 48 h and 72 h. Reagent grade xylose was also used as the control, since it was found that D-HMH predominantly consisted of xylose.

Chemical analysis of produced PHB using 2% D-HMH as the sole carbon source was analyzed using FT-IR and NMR spectroscopy and matched the proposed structure[24] (supplementary information).

Characterization of Extracted PHB

Cells were fed 2% D-HMH or xylose and fermented for either 48 h and 72 h. Then cells were isolated and dried followed by PHB extraction and purification. Feeding the cells with D-HMH yielded 1.69 g/L cell dry matter after 48 h incubation and 1.75 g/L cell dry matter after 72 h incubation. The control group showed a slightly faster growth rate at both times with cell dry weights equal to 1.88g/L after 48 h and 1.94 g/L after 72 h incubation (**Table 1.2**). In both groups, PHB was continually produced by cells, since its content in dry mass increased from 2.2% in 48 h to 4.8% in 72 h incubation. Although the PHB content increased by more than 100%, cell dry weights remained virtually unchanged in both groups. As a result, one could conclude that the cells are slowly metabolizing xylose and other available sugars to the required monomer, which takes longer than 48 h. This conclusion was further confirmed by molecular weight measurements of the PHB produced, where a drastic increase in average molecular weights after 72 h compared to 48 h incubation was found. These observations are also consistent with previous findings [25] describing low PHA accumulation rate in *E. coli* strain BL21.

Average molecular weight of the extracted PHB was determined by GPC. When D-HMH was used as carbon source, PHB molecular weight increased by 70% from 7.2 kDa after 48 h to 123 kDa after a 48 h or a 72 h incubation, respectively. Same trend was observed for the control group with 60% increase in molecular weight (**Table 1.2**). For the cells fed on D-HMH, polydispersity index (PDI) decreased from 1.4 after a 48 h fermentation to 1.3 after a 72 h fermentation. However, PDI remained unchanged for the control group. Overall, the molecular weights of PHB derived from D-HMH were slightly less than that of xylose, which could be attributed to presence of arabinose in hydrolysates. To study the effect of arabinose presented in

D-HMH, we used arabinose as the sole feedstock and analyzed the yielded PHB. Our studies show that arabinose can only yield low molecular weight oligomers (**Table 1.2**). This confirms the adverse effect of arabinose in D-HMH on the properties of the yielded PHB.

Table 1. 2: PHB production and physical properties of the products

Carbon source	Incubation time (h)	CDW (g/L)	PHB content (%CDW)	Mn (kDa)	Mw (kDa)	PDI	X_c (%) [a]
D-HMH	48	1.69±0.09	2.19±0.3	72	103	1.4	31.6
	72	1.75±0.07	4.84±0.7	123	166	1.3	44.8
Arabinose	48	1.56±0.09	1.67±0.4	5	6	1.2	2.4
Xylose (control)	48	1.88±0.06	2.27±0.3	88	115	1.3	34.2
	72	1.94±0.06	4.89±0.6	141	184	1.3	49.6

[a] Considering melting enthalpy of 100% crystalline poly hydroxybutyrate 146 J/g [26]

After the 48 h incubation period, D-HMH fed cells yielded PHB with 45% crystallinity, while control sample shows 50% crystallinity. After the 72 h incubation, the crystallinity increased by about 40% using both D-HMH and xylose, which corroborates with our molecular weight measurements and others previously reported results.[26] Since the sugar content of D-HMH mostly consists of xylose, one expects that the thermal properties should be in close proximity to the PHB derived from xylose-fed cells. However, we observed slightly lower thermal properties which could be attributed to the presence of arabinose in D-HMH since the arabinose-fed bacteria yielded low molecular weight PHBs with only 2.4% crystallinity and low thermal properties. Overall, xylose fed cells (control group) produced PHB with higher thermal stability and crystallinity, while the D-HMH fed cells produced PHB with thermal properties similar to that of control group (**Table S1. 1**) demonstrating the effectiveness of D-HMH for bacterial production of PHB with acceptable thermal properties for everyday applications such as packaging materials.[3] DSC thermograms and detailed thermal analysis of the yielded PHB could be found in supplementary information.

COCLUSION

This study demonstrates the possibility of using manure hydrolysates as the sole carbon source for bacterial production of PHB. It was found that manure hydrolysates contained mostly xylose and arabinose. The detoxification step successfully removed furans from hydrolysates yielding a carbon source with virtually no cell growth inhibitory effects. Physiological properties of the PHBs produced by engineered *E. coli,* fed by D-HMH, were studied, and found to be similar to the results from the control xylose-fed cells. These findings illustrate the potential use of manure hydrolysates as the sole carbon source for bacterial production of PHAs paving the road to a more efficient manure management via this waste-to-value approach.

SUPPORTING INFORMATION

Materials

Analytical grade xylose, arabinose, glucose, isopropyl-β- D-thiogalactoside (IPTG), furfural, and hydroxy methyl furfural (HMF) were purchased from Sigma-Aldrich. Reagent grade xylose and arabinose were purchased from Sigma-Aldrich. All other chemicals and reagents used in this study were analytical or reagent grade available in our lab stock. In all experiments, ultra-pure milli-Q water (18MΩ) was used.

Plasmid Construction

Escherichia coli BL21 (DE3) competent cells (New England BioLabs®) were used as the host strain for PHB production. A fragment containing phaCAB operon consisting of phaA (3-ketothiolase), phaB (acetoacetyl-CoA reductase), and phaC (PHA synthase) genes with their ribosomal binding sites, amplified from the R. eutropha H16 genomic DNA was designed according to the codon preferences of *E. coli*. The fragment was then inserted into pUC57 plasmid cloning vector isolated from *E. coli* strain DH5α with an ampicillin resistance marker and T7 promoter by Biomatik Corporation (Cambridge, Canada). Detailed information of the plasmid is provided in supplementary information. *E. coli* competent cells were transformed with the plasmid using heat shock according to manufacturer's protocol. Cells were then plated on Luria-Bertani (LB) agar media selection plate containing 50 μg/mL ampicillin and were incubated overnight at 37°C. The success of the process was confirmed by formation of colonies on an agar plate.

phaCAB Plasmid Sequence:

aattaatacgactcactataggggaattgtgagcggataacaattcccctctagaaataattttgtttaactttaagaaggagatatacatatggc
tactgggaaaggagccgccgccagcacccaggaaggcaaaagccaaccatttaaagtgaccccaggcccgttcgatcctgccacctggc
tggaatggtcacgtcaatggcaaggtacggagggcaacggccatgcggcagcgtccggcatccctgggcttgatgcactggctggtgtta
aaattgcgcctgcccaattgggagacatccaacagcgttatatgaaagatttttcggcgctgtggcaggcgatggcggaaggtaaagcaga
ggcgacgggaccgctgcatgaccgtcgctttgctggcgacgcctggcgtaccaatttgccctatcgttttgcggcagccttctacctgctgaa
cgctcgtgccctgactgagctggcagatgctgtcgaagcggatgccaaaacccgccaacgcatccgttttgccatctcacagtgggtcgac
gcaatgtcaccggccaacttcctggccaccaatccggaagcacagcgcctcctgattgaaagcggcggggaatcgctgcgcgccggcgt
tcgtaacatgatggaagatctgacccgtggtaagatttcgcagacggatgagtcggccttcgaggtgggtcgcaatgttgcagtgacagaa
ggcgcggtggtgtttgagaacgaatactttcaacttctccagtataaaccactgacggataaagtgcatgcgcgcccattgttaatggttcccc
cgtgcattaataaatactatatcctggatcttcagccggaaagctccttagtgcgccacgtggtggaacaggggcatactgtgtttttagttagc
tggcgcaatccagatgcctcaatggccggcagtacctgggatgactacattgaacacgcggctattcgcgcgatcgaagtggcacgcgac
atctcaggtcaggacaagattaacgtactcggcttttgcgtcggtggcactatcgtgagcaccgctctggcggtactggctgcgcgtggtga
acaccccgcagcgtcggttacgcttctgaccacactgttggatttcgccgacactggcatcttggatgtatttgtcgatgagggccacgttcag
ctgcgcgaggccactctgggtggcggcgccggcgcaccgtgcgctctgctgcgcggtctggagctcgcgaatacttttctttcttacgccc
gaacgatcttgtctggaattacgtagttgacaactatctcaaaggtaacacgcccgtgccgtttgatttattattctggaatggggatgcgacca
acctgccgggtccttggtattgttggtatctccgtcatacatacttacagaatgaattaaaggtcccaggtaaacttactgtgtgtggtgtcccgg
tagatctggcgagtatcgacgtgccgacctacatttatgggagtcgtgaagatcatattgtgccgtggaccgccgcgtacgcttctaccgcgc
ttctggcaaacaaattacgtttcgttctgggtgccagcggccacattgcgggtgttattaatcctccggccaaaaataaacgctcgcattggac
aaacgacgccttgccggagagccctcagcagtggttggcgggtgccattgagcaccatggaagttggtggccggactggacagcctggc
tggcgggccaagcaggcgcaaaacgcgctgcgccagccaactatggcaacgcgcgctaccgcgcgattgaacccgcgcctggccgct
atgtaaaagcaaaagcgtgacgcttgcatgagtgccggcgtgcgtcatgcacggcgccggcaggcctgcacgttccctcccgtttccattg
aaaggactacacaatgaccgatgttgttatcgtcagtgccgcgcgcaccgccgtgggtaaatttggcggcagtctggcgaaaatcccggcg
ccagaattgggcgcggtggtaatcaaagcggccctggaacgcgccggtgtgaaacctgagcaggtgagcgaagtaattatgggtcaggtt
ctgaccgcgggcagcgggcaaaatccggcgcgtcaggctgcgattaaggcaggccttccggcgatggtgcccgcgatgaccattaaca
aagtatgcggatcgggactgaaagcagtgatgctggccgctaacgccattatggcaggcgacgcggaaattgtggtcgctggcggacag
gagaatatgtcagccgcgcctcatgtgctgccgggtagccgcgacggctttcgcatgggtgatgcaaaactggtcgatactatgattgttga
cggcttatgggatgtgtacaaccagtaccacatgggcatcaccgccgagaacgtggccaaggaatacggcatcacacgcgaggcgcag
gatgagttcgccgtcggctcgcagaacaaggccgaagccgcgcagaaggccggcatgtttgacgaagagatcgtcccggtgctgatccc
gcagcgcaagggcgacccggtggccttcaagaccgacgagttcgtgcgccagggcgccacgctggacagcatgtccggcctcaagcc

cgccttcgacaaggccggcacggtgaccgcggccaacgcctcgggcctgaacgacggcgccgccgcggtggtggtgatgtcggcggc
caaggccaaggaactgggcctgaccccgctggccacgatcaagagctatgccaacgccggtgtcgatcccaaggtgatgggcatgggc
ccggtgccggcctccaagcgcgccctgtcgcgcgccgagtggaccccgcaagacctggacctgatggagatcaacgaggcctttgccg
cgcaggcgctggcggtgcaccagcagatgggctgggacacctccaaggtcaatgtgaacggcggcgccatcgccatcggccacccgat
cggcgcgtcgggctgccgtatcctggtgacgctgctgcacgagatgaagcgccgtgacgcgaagaagggcctggcctcgctgtgcatcg
gcggcggcatgggcgtggcgctggcagtcgagcgcaaataaggaaggggttttccggggccgcgcgcggttggcgcggacccggcg
acgataacgaagccaatcaaggagtggacatgactcagcgcattgcgtatgtgaccggcggcatgggtggtatcggaaccgccatttgcc
agcggctggccaaggatggctttcgtgtggtggccggttgcggccccaactcgccgcgccgcgaaaagtggctggagcagcagaaggc
cctgggcttcgatttcattgcctcggaaggcaatgtggctgactgggactcgaccaagaccgcattcgacaaggtcaagtccgaggtcggc
gaggttgatgtgctgatcaacaacgccggtatcacccgcgacgtggtgttccgcaagatgacccgcgccgactgggatgcggtgatcgac
accaacctgacctcgctgttcaacgtcaccaagcaggtgatcgacggcatggccgaccgtggctggggccgcatcgtcaacatctcgtcg
gtgaacgggcagaagggccagttcggccagaccaactactccaccgccaaggccggcctgcatggcttcaccatggcactggcgcagg
aagtggcgaccaagggcgtgaccgtcaacacggtctctccgggctatatcgccaccgacatggtcaaggcgatccgccaggacgtgctc
gacaagatcgtcgcgacgatcccggtcaagcgcctgggcctgccggaagagatcgcctcgatctgcgcctggttgtcgtcggaggagtc
cggtttctcgaccggcgccgacttctcgctcaacggcggcctgcatatgggctgacctgc

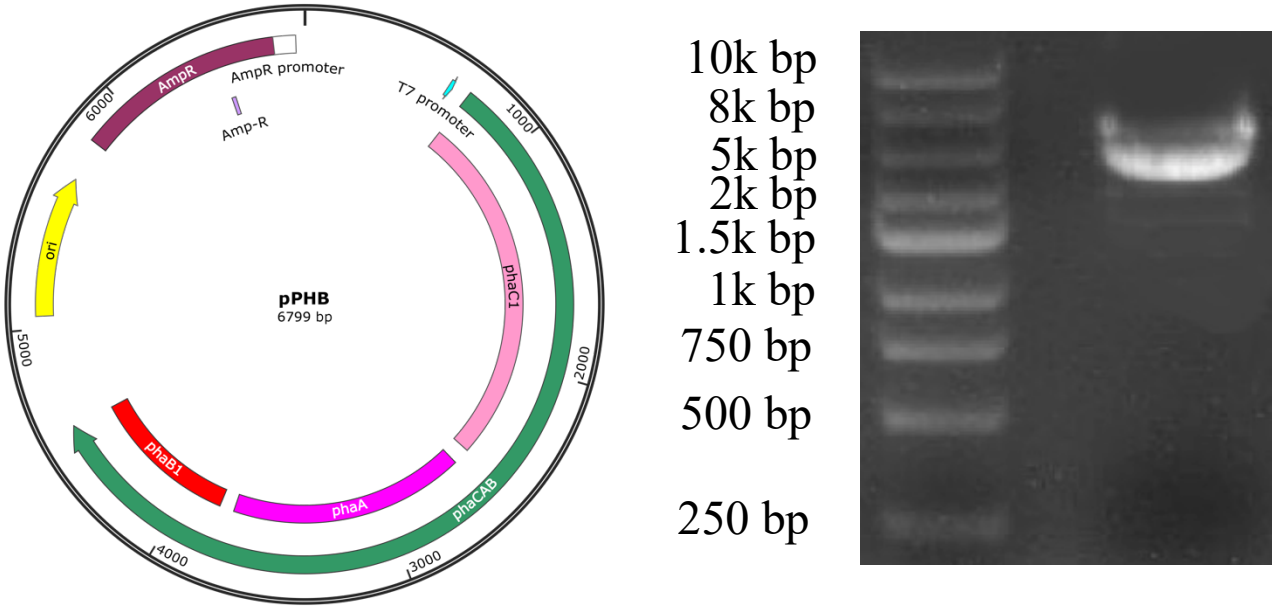

Figure S1. 1 (left) pPHB plasmid map harboring phaCAB operon and (right) agarose electrophoresis gel run for constructed plasmid.

Chemical Structure of the PHB

^{1}HNMR (500 MHz, $CDCl_3$) spectra also confirms the proposed structure of the isolated polymer (PHB) as δ (ppm): 7.26 (Chloroform-d), 5.20 (m, 1H), 2.51 (d, 1H), 2.41 (d, 1H), and 1.21 (d, 3H).

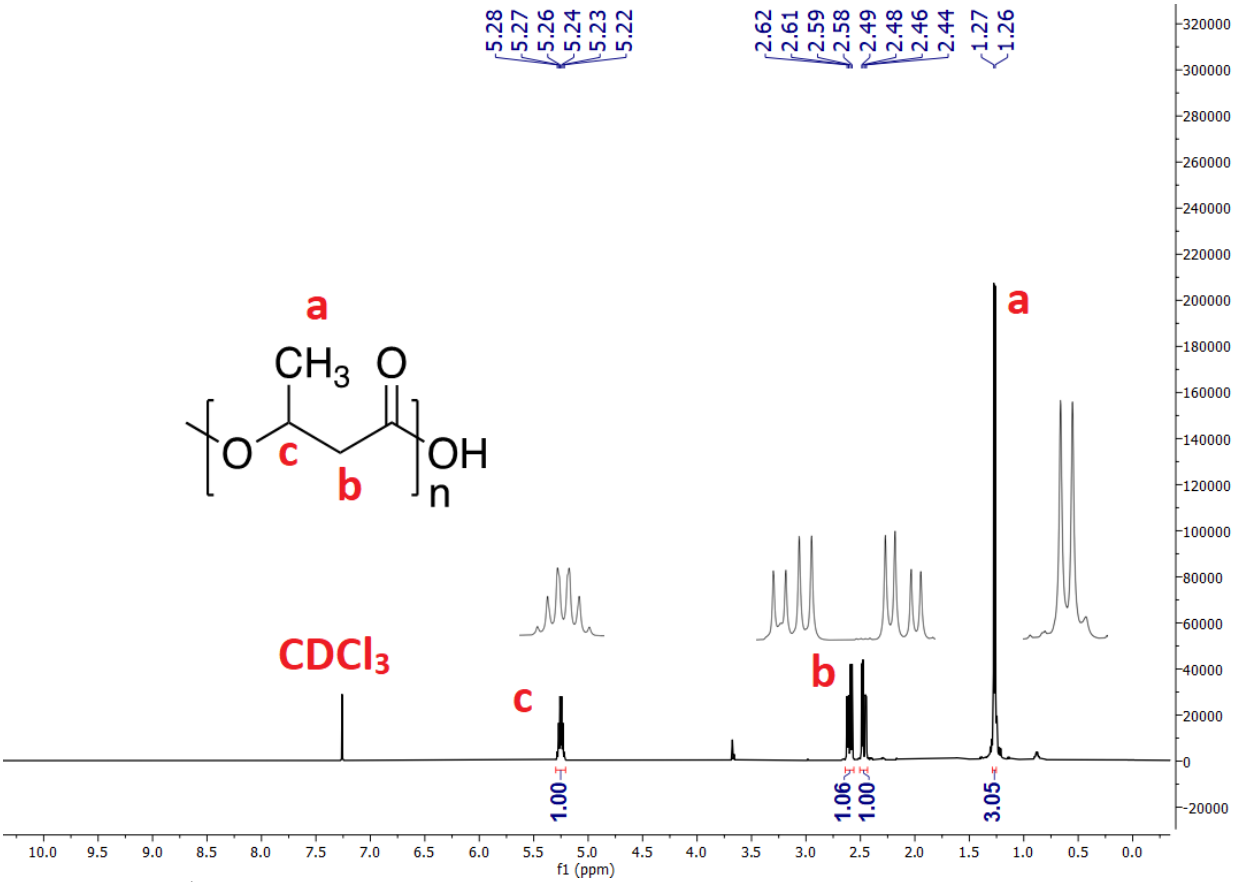

Figure S1. 2: ^{1}H NMR spectrum in $CDCl_3$ of PHB derived from cells on D-HMH after 72 h

The FT-IR spectra (**Fig S1. 2**) exhibited characteristic bands for the ester bonds which are visible at 1028 cm^{-1} (O-C-C stretch), 1260 cm^{-1} (C-C-O stretch), and 1724 cm^{-1} (C=O stretch). In addition, the bands at 1380 cm^{-1}, 1458 cm^{-1}, and 2922 cm^{-1} indicated CH_3, -CH_2, and -CH groups, respectively.

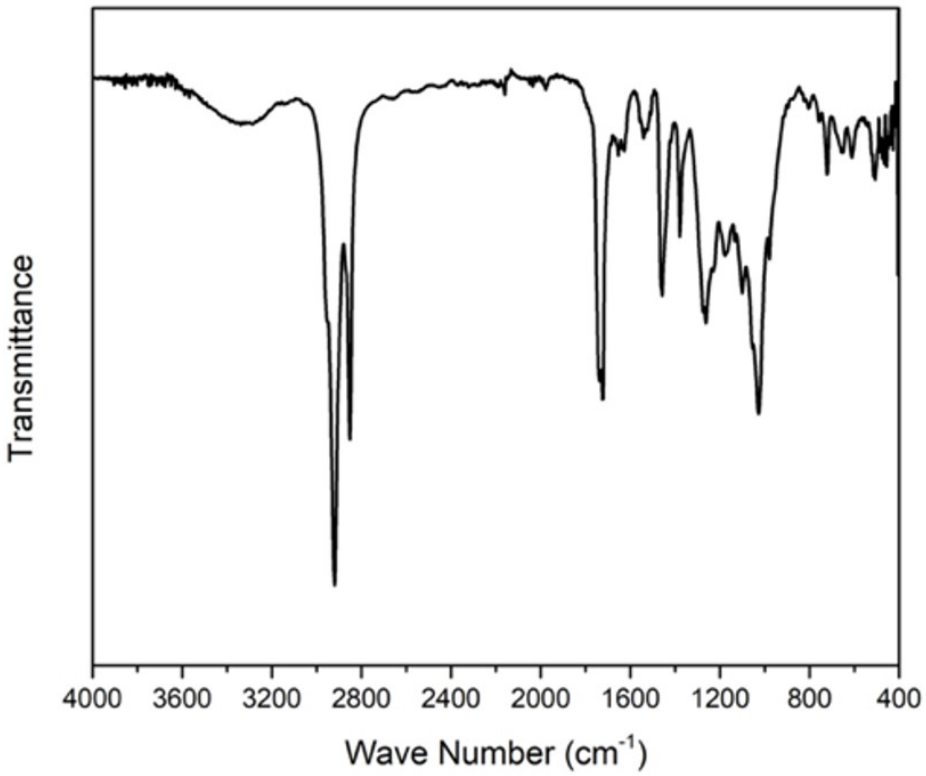

Figure S1. 3: FT-IR spectrum of PHB derived from cells on D-HMH after 72 h.

Thermal Analysis

The DSC tests were performed at a heating rate of 10°C/min in a nitrogen atmosphere at temperatures ranging from -50 to 275 °C. The samples were heated from 25 to 150 °C and then cooled to -50 °C, to erase the thermal history. At the final heating stage, the samples were heated from -40 to 275 °C and the resulting thermographs are depicted in (**Fig S1. 4).** Upon an increase in incubation time, all the samples demonstrated an increase in molecular weights, regardless of feedstock. Therefore, T_g, T_m, and T_d have all shifted to higher temperatures (**Table S1.1**); due to the increase in molecular interactions between the chains and a decrease in chain mobility. The melting enthalpy was increased from 46.2 J/mol after the 48 h incubation to 68.4 J/mol after 72 h for the PHB yielded from D-HMH. A similar change was also observed for the control group with an increase from 49.9 J/mol after 48 h to 71.4 J/mol after 72 h.

Table S1. 1: Thermal properties of the extracted PHB.

Carbon source	Incubation time (h)	T_g (°C)	T_m (°C)	T_d (°C)	ΔH_m (J/g)	[a] X_c (%)
D-HMH	48	3.5	171.7	191.0	46.2	31.6
	72	4.3	177.0	204.6	68.4	44.8
Xylose (control)	48	3.6	172.7	193.9	49.9	34.2
	72	5.9	180.2	213.9	71.4	49.6
Arabinose	48	1.1	155.7	190.7	3.6	2.4

[a] Considering melting enthalpy of 100% crystalline poly hydroxybutyrate 146 J/g

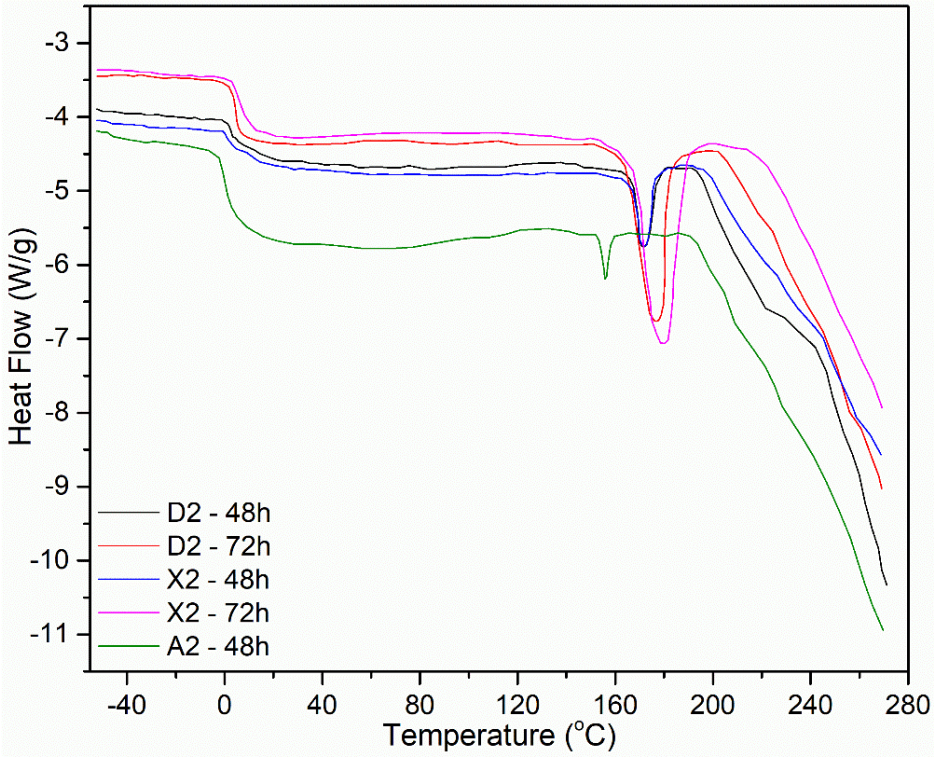

Figure S1. 4: DSC thermograms of produced PHB using D2 (2% W/V D-HMH), X2 (2% W/V xylose), and A2 (2% W/V arabinose) as carbon source at designated timeframes.

REFERENCES

(1) Geyer, R.; Jambeck, J. R.; Law, K. L. Production, Use, and Fate of All Plastics Ever Made. *Science advances* **2017**, *3* (7), e1700782.

(2) *Biotechnological Applications of Polyhydroxyalkanoates*; Kalia, V. C., Ed.; Springer Singapore, 2019. https://doi.org/10.1007/978-981-13-3759-8.

(3) Bugnicourt, E.; Cinelli, P.; Lazzeri, A.; Alvarez, V. A. Polyhydroxyalkanoate (PHA): Review of Synthesis, Characteristics, Processing and Potential Applications in Packaging. **2014**.

(4) Choi, S. Y.; Rhie, M. N.; Kim, H. T.; Joo, J. C.; Cho, I. J.; Son, J.; Jo, S. Y.; Sohn, Y. J.; Baritugo, K.-A.; Pyo, J. Metabolic Engineering for the Synthesis of Polyesters: A 100-Year Journey from Polyhydroxyalkanoates to Non-Natural Microbial Polyesters. *Metabolic engineering* **2020**, *58*, 47–81.

(5) Leong, Y. K.; Show, P. L.; Ooi, C. W.; Ling, T. C.; Lan, J. C.-W. Current Trends in Polyhydroxyalkanoates (PHAs) Biosynthesis: Insights from the Recombinant Escherichia Coli. *Journal of biotechnology* **2014**, *180*, 52–65.

(6) Favaro, L.; Basaglia, M.; Casella, S. Improving Polyhydroxyalkanoate Production from Inexpensive Carbon Sources by Genetic Approaches: A Review. *Biofuels, Bioproducts and Biorefining* **2019**, *13* (1), 208–227.

(7) Rodriguez-Perez, S.; Serrano, A.; Pantión, A. A.; Alonso-Fariñas, B. Challenges of Scaling-up PHA Production from Waste Streams. A Review. *Journal of environmental management* **2018**, *205*, 215–230.

(8) Raza, Z. A.; Tariq, M. R.; Majeed, M. I.; Banat, I. M. Recent Developments in Bioreactor Scale Production of Bacterial Polyhydroxyalkanoates. *Bioprocess and biosystems engineering* **2019**, *42* (6), 901–919.

(9) Perez-Rivero, C.; López-Gómez, J. P.; Roy, I. A Sustainable Approach for the Downstream Processing of Bacterial Polyhydroxyalkanoates: State-of-the-Art and Latest Developments. *Biochemical Engineering Journal* **2019**, *150*, 107283.

(10) Kumar, M.; Rathour, R.; Singh, R.; Sun, Y.; Pandey, A.; Gnansounou, E.; Lin, K.-Y. A.; Tsang, D. C.; Thakur, I. S. Bacterial Polyhydroxyalkanoates: Opportunities, Challenges, and Prospects. *Journal of Cleaner Production* **2020**, 121500.

(11) Sasikumar, C.; Sundaresan, R.; Nagaraja, M.; Rajaganapathy, C. A Review on Energy Generation from Manure Biomass. *Materials Today: Proceedings* **2020**.

(12) Altun, M. Polyhydroxyalkanoate Production Using Waste Vegetable Oil and Filtered Digestate Liquor of Chicken Manure. *Preparative biochemistry & biotechnology* **2019**, *49* (5), 493–500.

(13) Bhati, R.; Mallick, N. Carbon Dioxide and Poultry Waste Utilization for Production of Polyhydroxyalkanoate Biopolymers by Nostoc Muscorum Agardh: A Sustainable Approach. *Journal of applied phycology* **2016**, *28* (1), 161–168.

(14) Coats, E. R.; Watson, B. S.; Brinkman, C. K. Polyhydroxyalkanoate Synthesis by Mixed Microbial Consortia Cultured on Fermented Dairy Manure: Effect of Aeration on Process Rates/Yields and the Associated Microbial Ecology. *Water research* **2016**, *106*, 26–40.

(15) Hanson, A. J.; Guho, N. M.; Paszczynski, A. J.; Coats, E. R. Community Proteomics Provides Functional Insight into Polyhydroxyalkanoate Production by a Mixed Microbial Culture Cultivated on Fermented Dairy Manure. *Applied microbiology and biotechnology* **2016**, *100* (18), 7957–7976.

(16) Wei, L.; Guho, N. M.; Coats, E. R.; McDonald, A. G. Characterization of Poly (3-hydroxybutyrate-co-3-hydroxyvalerate) Biosynthesized by Mixed Microbial Consortia Fed Fermented Dairy Manure. *Journal of Applied Polymer Science* **2014**, *131* (11).

(17) Ahn, J.; Jho, E. H.; Nam, K. Effect of C/N Ratio on Polyhydroxyalkanoates (PHA) Accumulation by Cupriavidus Necator and Its Implication on the Use of Rice Straw Hydrolysates. *Environmental Engineering Research* **2015**, *20* (3), 246–253.

(18) Zhang, Y.; Xia, C.; Lu, M.; Tu, M. Effect of Overliming and Activated Carbon Detoxification on Inhibitors Removal and Butanol Fermentation of Poplar Prehydrolysates. *Biotechnology for biofuels* **2018**, *11* (1), 1–14.

(19) Lee, D.-J.; Yim, J. H.; Jung, S.; Jang, M.-S.; Jeong, G.-T.; Jeong, K.-H.; Lee, D.-H.; Kim, J. K.; Tsang, Y. F.; Jeon, Y. J. Valorization of Animal Manure: A Case Study of Bioethanol Production from Horse Manure. *Chemical Engineering Journal* **2021**, *403*, 126345.

(20) Martinez, A.; Rodriguez, M. E.; York, S. W.; Preston, J. F.; Ingram, L. O. Use of UV Absorbance to Monitor Furans in Dilute Acid Hydrolysates of Biomass. *Biotechnology progress* **2000**, *16* (4), 637–641.

(21) Takisawa, K.; Ooi, T.; Matsumoto, K.; Kadoya, R.; Taguchi, S. Xylose-Based Hydrolysate from Eucalyptus Extract as Feedstock for Poly (Lactate-Co-3-Hydroxybutyrate) Production in Engineered Escherichia Coli. *Process Biochemistry* **2017**, *54*, 102–105.

(22) Pan, W.; Perrotta, J. A.; Stipanovic, A. J.; Nomura, C. T.; Nakas, J. P. Production of Polyhydroxyalkanoates by Burkholderia Cepacia ATCC 17759 Using a Detoxified Sugar Maple Hemicellulosic Hydrolysate. *Journal of Industrial Microbiology and Biotechnology* **2012**, *39* (3), 459–469.

(23) Ahn, J.; Jho, E. H.; Kim, M.; Nam, K. Increased 3HV Concentration in the Bacterial Production of 3-Hydroxybutyrate (3HB) and 3-Hydroxyvalerate (3HV) Copolymer with Acid-Digested Rice Straw Waste. *Journal of Polymers and the Environment* **2016**, *24* (2), 98–103.

(24) Mostafa, Y. S.; Alrumman, S. A.; Alamri, S. A.; Otaif, K. A.; Mostafa, M. S.; Alfaify, A. M. Bioplastic (Poly-3-Hydroxybutyrate) Production by the Marine Bacterium Pseudodonghicola Xiamenensis through Date Syrup Valorization and Structural Assessment of the Biopolymer. *Scientific Reports* **2020**, *10* (1), 8815. https://doi.org/10.1038/s41598-020-65858-5.

(25) Gao, D.; Luan, Y.; Wang, Q.; Liang, Q.; Qi, Q. Construction of Cellulose-Utilizing Escherichia Coli Based on a Secretable Cellulase. *Microbial Cell Factories* **2015**, *14* (1), 1–8.

(26) Chan, C. H.; Kummerlöwe, C.; Kammer, H.-W. Crystallization and Melting Behavior of Poly (3-hydroxybutyrate)-based Blends. *Macromolecular Chemistry and Physics* **2004**, *205* (5), 664–675.

Chapter 2: Analysis of Degradation

Mechanism and Kinetics of Enzymatic Degradation of Polyester Microparticles Using a Shrinking Particle-Shrinking Core Model

ABSTRACT

Generalized shrinking particle (SPM) and shrinking core (SCM) models were developed to the kinetics of heterogenous enzymatic degradation of polymer microparticles in a continuous microflow system. This enzymatic degradation was performed in a microfluidic device designed to both physically separate and immobilize the microparticles. Then time-resolved measurements were made using image processing of the physical changes of the particles during degradation. The kinetics of enzyme-polymer intermediate formation, enzymatic bond cleavage, and enzyme diffusion through the layer of degraded substrate (SCM only) were mathematically derived to predict the time-resolved degradation of the substrate. The proposed models were tested against the degradation of 15-25 μm particles of polycaprolactone (PCL) and poly (butylene adipate-co-terephthalate) (PBAT) by cutinase enzyme from *Humicola insolens*. Degradation of PCL microparticles followed the SPM model and its kinetics were found to be zero-order, while the SCM model applied to PBAT microparticles showed first-order kinetics. Further, the degradation of polybutylene succinate (PBS), and poly butylene-sebacate–co–terephthalate (PBSeT) microparticles demonstrated wide applicability of the method. The use of image processing simplifies the required analysis by eliminating the need to remove aliquots or concentrate effluent for additional analytical characterization.

Keywords: Shrinking particle; Shrinking core; Enzymatic degradation; Degradation kinetics; Microfluidics; First-order; Zero-order

INTRODUCTION

Over the past few decades, environmental issues arising from the use and disposal of non-biodegradable polymers have become a worldwide concern for the scientific community, general public, and legislators. To address these concerns, researchers have been working to

develop biodegradable polymers and understand the mechanisms involved in their biodegradation. General biodegradation mechanisms that occur through heterogeneous enzymatic degradation involves extracellular enzymes which break polymer chains into shorter pieces which can then be catabolized and become more bioavailable.[1] The first aspect of heterogeneous enzymatic degradation typically consists of four steps: (1) diffusion of the enzyme through the bulk solution to the surface of the substrate; (2) anchoring of the enzyme's active sites to the degradable bonds of the substrate forming a polymer-enzyme active intermediate; (3) catalytic hydrolysis of the bond; and (4) diffusion of degraded materials back to the bulk solution.[2] Each of these steps can affect the overall process where the slowest step is rate determining (RDS). Agitation is used in bulk systems to simplify the process and eliminate steps 1 and 4, because agitation is thought to increase the collision between enzyme molecules and the substrate. However, the impact of agitation on the kinetics of the degradation is not well understood, and the lack of uniform agitation conditions makes it difficult to compare the results from one study to the next. Furthermore, agitation can adversely affect degradation kinetics by lowering, or completely obscuring, autocatalytic effects.[3] Also, physiological phenomena associated with enzymatic degradation of polymers in nature are known to be slow processes,[4] therefore, static or slow agitation conditions have been suggested to study the enzymatic degradation of such polyesters.[5]

Microfluidic techniques have been used to study polymer degradation on the microscale providing a slow or close-to-static flow of enzyme solution over the substrate.[6–11] The second advantage of microfluidic techniques over degradation in agitated bulk systems is the constant introduction of fresh enzyme to the system removing the effect of enzyme deactivation throughout the process. Enzyme deactivation is an aspect of degradation kinetics which has not

been deeply investigated. Previously, we developed a microfluidic device to qualitatively study the enzymatic degradation of a single poly (butylene adipate-co-terephthalate) (PBAT) microparticle.[4] Here we use a similar technique by designing a microfluidic device to study the degradation kinetics of a group of polymer microparticles. Because the associated transport phenomena in a continuous flow system is substantially different, kinetic models developed for bulk systems with agitation cannot be used. Therefore, in addition to developing a continuous flow device to study degradation kinetics, we also developed generalized mathematical models to describe heterogenous enzymatic degradation phenomenon in a continuous system with laminar flow.

Several studies have been focused on the development of a degradation model for water-insoluble polymers. A simple two-step degradation kinetic model similar to the Michaelis-Menten model has been proposed for enzymatic degradation of polyhydroxy butyrate (PHB) particles,[12] and other polymers.[13,14] This mathematical model assumes a homogenous process even though the polymer substrate is insoluble, and thus it cannot be used to predict what quantity of polymer degrades over time. The equation was then modified to address both the effect of enzyme concentration and the heterogeneity of the substrate.[1] However, because only the initial degradation rate was measured, no relationship was found between the particle's diameter and its rate of degradation.[1]

A different generalized model describing simultaneous autocatalytic and non-autocatalytic reactions [15] was used to study the kinetics of polymer degradation.[16–18] In these studies the autocatalytic and non-autocatalytic processes were not clearly defined and the enzyme is considered solely as the catalyst.[1] Ultimately, this model was found to be more suitable for non-enzymatic, thermal, and mechanical degradation of polymers.

Shrinking Particle (SPM) and Shrinking Core (SCM) models are widely used to describe transport phenomena in solid-fluid chemical reactions,[19–25] including polymer degradation.[26–31] These models by themselves can describe homogenous acid or base hydrolysis of polyethylene terephthalates, but cannot accurately describe the multi-step heterogenous enzymatic degradation of polymers. We postulated that a combined Shrinking Particle (SPM) - Shrinking Core (SCM) model which accounts for each step involved in polymer degradation would more accurately reflect the enzymatic degradation kinetics of polymer microparticles, compared with previously developed kinetic models. Hence, we sought to develop these two models in tandem to describe enzymatic degradation kinetics more accurately.

To achieve our goal, the shape and morphology of the polymer microparticles were monitored during the degradation process using a microfluidic platform with crescent-shape traps which separated and immobilized a statistical number microparticles. Two key advantages of using a microfluidic platform include: time resolved data; and the ability to measure morphological changes in the substrate using quick, simple, and inexpensive image processing methods.

Microparticles of polycaprolactone (PCL), poly (butylene adipate-co-terephthalate) (PBAT), poly (butylene sebacate-co-terephthalate) (PBSeT), and polybutylene succinate (PBS) were prepared via an oil-in-water solvent removal method. A high-quality statistical sample of particles (10-20), limited by the microscope's view field, was monitored in real-time during degradation by a cutinase enzyme from *Humicola insolens* which efficiently degrades a wide range of polyesters.[32] Image processing was used to assess the morphological changes (size or darkness) and find the RDS. This data was then used to calculate the kinetic parameters. We show that the proposed model for studying polymer microparticle enzymatic degradation on a

microfluidic platform is a viable method for assessing enzymatic degradation of water-insoluble polymers.

MATHEMATICAL MODELS

Kinetic Model

To develop a mathematical model and measure the kinetics of degradation, the reaction steps must be identified first. Non-catalytic hydrolysis of the polymers studied here was not measurable. Thus, the enzymatic degradation can be described as a two-step process (**Eq. 1**) where a complex between the enzyme molecules and the polymers' surface (*EP*) is formed, and then *EP* cleaves the ester bonds on the surface producing degraded materials (**Eq. 2**). This two-step process is analogous to previous studies.[12, 14]

$$\varepsilon E(aq) + P(s) \overset{K}{\rightleftharpoons} EP \quad \textbf{(1)}$$

$$EP \overset{k}{\rightarrow} D \quad \textbf{(2)}$$

Where *E* is the enzyme present in the solution with the concentration of [E], *P* is the polymer, *D* is the degraded material, *K* is the equilibrium constant for *EP* and is equal to $\frac{K_1}{K_{-1}}$, *k* is the catalytic rate constant of *D* formation and ε is the stoichiometric coefficient.

A general Shrinking Particle Model (SPM) and a Shrinking Core Model (SCM) are proposed (**Fig 2. 1**) for heterogenous enzymatic degradation of polymer microparticles. The kinetics of each step is mathematically derived assuming they are the rate determining step (RDS). We show the derivation of the governing equation of degradation kinetics if more than one step significantly contributes to the kinetics of degradation.

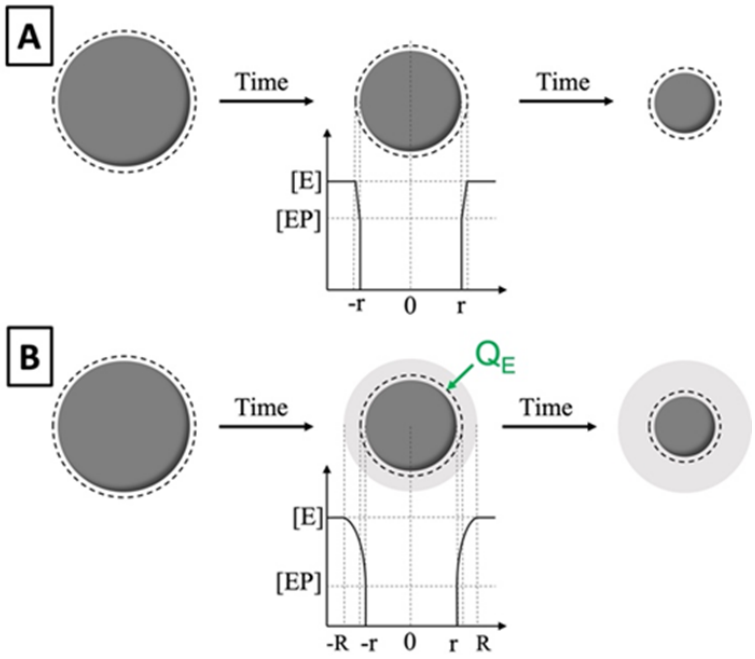

Figure 2. 1: A) Shrinking Particle Model Scheme; A monolayer of intermediate EP (dashed line) is formed on the surface of the particle (solid circle). This layer then transforms to degraded materials. **B)** Shrinking Core Model. A layer of degraded material (light gray) is formed around the unreacted core (dark gray). The total size of the particle remains unchanged while the core continues to shrink as degradation continues, similar to SPM model. Q_E is the flux of enzyme diffusion through the degraded layer.

Shrinking Particle Model (SPM)

During degradation, the polymer segments in contact with enzyme molecules break into increasingly smaller pieces which eventually degrade to hydrophilic oligomers and monomers. In the SPM model, particles continue to shrink as the enzymatic degradation progresses, resulting in a constant reduction of the particle size until full degradation is achieved (**Fig 2. 1A**). This model is similar to the surface erosion model, where the high crystallinity and hydrophobicity limits the water and enzyme's ability to penetrate through to the core of the particle such that degradation occurs from the surface progressively toward the core.[33] In contrast to the surface erosion model, the SPM model suggests that this phenomenon may arise from the increased solubility of the

degraded materials into the surrounding aqueous media leaving the unreacted core of the particle exposed to its surrounding.

From a mechanistic point of view, enzyme molecules form a monolayer on the substrate's surface producing intermediate *EP* (**Eq. 1**). If this step is slower than the polymer's conversion to degraded materials, it is the RDS; we will refer to this as the *EP control* mechanism. Assuming steady-state conditions for enzyme-substrate interaction,[34] all the *EP* formed (N_{EP}) is instantly converted to the degraded material and its net concentration is equal to zero at any given time. Thus, the moles of the polymer consumed is equal to that of consumed *E* and the overall reaction scheme transforms to the following:

$$\varepsilon E(aq) + P(s) \overset{K_1}{\rightarrow} D \qquad \textbf{(3)}$$

$$-\varepsilon \mathrm{r_P} = -\mathrm{r_E} \text{ where } -\varepsilon \frac{d}{dt} N_P = -\frac{d}{dt} N_E \qquad \textbf{(4)}$$

Where r_p and r_E are the rate of consumption of the polymer and enzyme, respectively. Assuming equation **(4)** represents an elementary reaction, the rate of consumption of *E* could be written as the following:

$$-\varepsilon \frac{1}{A_P} \frac{dN_P}{dt} = -\frac{1}{A_P} \frac{dN_E}{dt} = K_1[E]^{\varepsilon} \qquad \textbf{(5)}$$

Where A_p is the surface area of the particle and N_p and N_E represent the amount of polymer and enzyme, respectively. Since the reaction takes place on the surface, we write its kinetics according to the surface A_P:

$$-\frac{\varepsilon}{A_P} \frac{d}{dt} N_P = -\frac{\varepsilon}{4\pi r^2} \frac{d}{dt} N_P = -\frac{\varepsilon}{4\pi r^2} 4\rho\pi r^2 \frac{d}{dt} r = -\varepsilon\rho \frac{d}{dt} r \qquad \textbf{(6)}$$

Where r is the radius of the particle at any given time t, and ρ is the density of the polymer. Combining equations (**5**) and (**6**), the degradation kinetics can be expressed as:

$$-\varepsilon\rho\frac{d}{dt}r = K_1[E]^{\varepsilon} \quad \textbf{(7)}$$

$$-\int_R^r dr = \frac{K_1[E]^{\varepsilon}}{\varepsilon\rho}\int_0^t dt \quad \textbf{(8)}$$

Solving equation **(8)** and rearranging for time provides:

$$t_{EP} = \tau_{EP}\left[1-\left(\frac{r}{R}\right)\right] \text{ where } \tau_{EP} = \frac{\varepsilon\rho R}{K_1[E]^{\varepsilon}} \quad \textbf{(9)}$$

In equation **(9)**, R is the initial radius of the particle and τ is the time required for the full degradation (characteristic time). The direct relationship between τ and R in the degradation of a substrate has been previously observed in other reaction kinetics.[21,35]

If equation **(2)** is the RDS, the formation of the *EP* layer is faster than its consumption;[34] the amount of degraded polymer is equal to that of the *EP* converted to *D*. In other words, the rate of bond cleavage in the polymer backbone dominates the kinetics of degradation. We will refer to this as the *RXN control* mechanism. Subsequently:

$$-r_P = -r_{EP} \text{ where } -\frac{d}{dt}N_{EP} = \frac{d}{dt}N_D \quad \textbf{(10)}$$

$$\frac{d}{dt}N_D = k\,[EP] \quad \textbf{(11)}$$

Considering the equilibrium in equation **(1)**:

$$\frac{d}{dt}N_D = k\,K[E]^{\varepsilon} \quad \textbf{(12)}$$

According to the quasi steady-state approximation of enzymatic reactions,[34] the concentration of *EP* is always constant at any given time, however, N_{EP} changes as the A_P shrinks, consequently:

$$N_{EP} = A_P \emptyset \quad \textbf{(13)}$$

$$-\frac{d}{dt} N_{EP} = -8\emptyset\pi r \frac{dr}{dt} \quad \textbf{(14)}$$

Where $\emptyset$ is the enzyme loading per unit of the polymer surface (mole/area) and is a function of [E]. Previous studies reported that the immobilization of enzyme onto the polymer surface follows Langmuir isotherm kinetics,[36] thus:

$$N_{EP} = A_P \emptyset_{max} \frac{K[E]}{1+K[E]} \quad \textbf{(15)}$$

where $\emptyset_{max}$ is the maximum enzyme loading onto the surface. Combining equations (**12**), (**14**), and (**15**) the kinetics of *EP* consumption can therefore be expressed as follows:

$$-8\pi\emptyset_{max} \frac{K[E]}{1+K[E]} \, r \frac{dr}{dt} = kK[E]^{\varepsilon} \quad \textbf{(16)}$$

$$-\int_R^r r \, dr = \frac{k[E]^{\varepsilon-1}(1+K[E])}{8\pi\emptyset_{max}} \int_0^t dt \quad \textbf{(17)}$$

Previous measurements of K [1] demonstrated that K[E]<<1, and consequently 1+ K[E] is approximately 1. By solving equation **(17)** and rearranging we get an expression for the time and conversion (r/R):

$$t = \tau\left[1 - \left(\frac{r}{R}\right)^2\right] \text{ where } \tau = \frac{A_0\emptyset_{max}}{k[E]^n} \quad \textbf{(18)}$$

In equation **(18)**, A_0 is the initial surface area of the particle and $n = \varepsilon - 1$. The direct relation of τ_{RXN} and A_0 in equation **(18)** is analogous to a model reported previously.[31] The measurement of

enzyme loading in previous studies was reported as 0.25 ng cm^{-2}.[37] To simplify the calculations, an apparent rate coefficient *k'* is assumed and equation **(18)** transforms to the following:

$$k' = \frac{k}{\emptyset_{max}} \quad \textbf{(19)}$$

$$t_{RXN} = \tau_{RXN}\left[1 - \left(\frac{r}{R}\right)^2\right] \text{ where } \tau_{RXN} = \frac{A_0}{k'[E]^n} \quad \textbf{(20)}$$

Shrinking Core Model (SCM)

The shrinking core model (SCM) applies to particles where microparticle size is not affected by the degradation reaction; the particles maintain their initial shape and size during the degradation. This mode of degradation is similar to bulk degradation [33] also known as the progressive conversion model, with a substantial difference. In the bulk degradation mechanism, the enzyme molecules penetrate through the surface of the particle to the core and no gradient of enzyme concentration within the particle is assumed.[33] Because of these assumptions, the bulk degradation model only applies to highly porous particles. The shrinking core model addresses this issue assuming an unreacted core above which a stable layer of degraded materials, *D,* is formed, which we refer to as the ash layer. No enzyme penetration through the surface of the unreacted core is assumed, however enzyme does penetrate the ash layer, the thickness of which increases over time **(Fig 2. 1B)**.

The SCM mechanism for degradation remains similar to the SPM such that equations **(1)** and **(2)** apply to the SCM, therefore, equations (**9**) and (**20**) apply to this model as well. However, since the enzyme molecules must diffuse through the ash layer to reach to the core's surface, a gradient in enzyme concentration inside the ash layer must be considered **(Fig 2. 1B)**.

Assuming the steady state condition, the rate of change of [E] (dN_E) is equal to its rate of diffusion through the ash layer. A previously reported model for gas-solid reactions describes the diffusion of reactants through the ash layer.[38] This model is also applicable for liquid-solid reactions if the velocity ratio (liquid flow rate over solid's shrinkage rate) is larger than unity. In experiments performed in microfluidic devices, the flow velocity and the particles' shrinkage rate were calculated to be 0.1 m h^{-1} and maximum 25 μm h^{-1}, respectively. Thus, the velocity ratio is several orders of magnitude larger than unity. As a result, a previously reported formulae for gas-solid reactions can also be used here.[35] Assuming the diffusion follows Fick's law:

$$-\varepsilon \frac{d}{dt} N_P = -\frac{d}{dt} N_E = 4\pi r^2 Q_E \quad \textbf{(21)}$$

$$Q_E = \mathcal{D} \frac{d[E]}{dr} \quad \textbf{(22)}$$

In equation (**22**), $\mathcal{D}$ is the diffusion coefficient of enzyme molecules through the ash layer and Q_E is the flux of diffusion. By combining equations (**21**) and (**22**):

$$-\frac{d}{dt}\ N_E = 4\pi r^2 \mathcal{D} \frac{d[E]}{dr} \quad \textbf{(23)}$$

Integration of equation (**23**) across the ash layer shows that at any given time, dN_E is constant and proportional to the diffusion coefficient $\mathcal{D}$.

$$-\frac{d}{dt} N_E \left(\frac{1}{r} - \frac{1}{R}\right) = 4\pi \mathcal{D}[E] \quad \textbf{(24)}$$

Combining equations (**6**), (**21**), (**23**) and (**24**) will result in the following:

$$-\varepsilon\rho \int_R^r \left(\frac{1}{r} - \frac{1}{R}\right) r^2\, dr = \mathcal{D}[E] \int_0^t dt \quad \textbf{(25)}$$

Solving equation (**25**) and rearranging provides an expression for the kinetics of SCM degradation if diffusion is the RDS:

$$t_{\mathcal{D}} = \tau_{\mathcal{D}}\left[1 - 3\left(\frac{r}{R}\right)^2 + 2\left(\frac{r}{R}\right)^3\right] \text{ where } \tau_{\mathcal{D}} = \frac{\varepsilon\rho R^2}{6\mathcal{D}[E]} \quad \textbf{(26)}$$

To elucidate the degradation kinetics, the characteristic time (τ) and its relation to the particle size (R) must first be found to identify the RDS. The experimental time-conversion data (r/R vs. t) for particles with different radii should be fitted with possible RDS models at a certain enzyme concentration. Note that the conversion is defined as the radius of the particle (SPM), or unreacted core (SCM) normalized to their initial value (r/R).

Once the RDS is found, the kinetic parameters K, k', n, and $\mathcal{D}$ can be calculated by finding the relation between τ and [E] (**Eqs. 9, 20, and 26**). In this regard, degradation of particles should be performed using enzyme at different concentrations and the characteristic time and enzyme concentration data (τ vs. [E]) fitted to the associated RDS model. Notably, in the SCM mechanism, if diffusion affects the degradation kinetics alongside another RDS, then the time-conversion relationship can be assumed as the combination of diffusion and the other effective step. A summary of SPM-SCM model, associated RDSs, and typical conversion-time graphs are provided in **Table S2. 1** and **Fig S2. 1**, respectively.

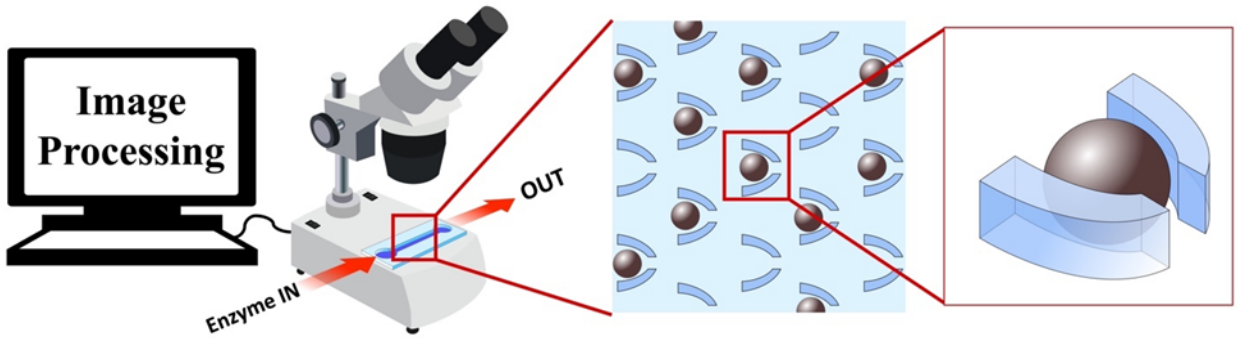

Figure 2. 2: Schematics of experimental setup and the structure of microfluidic device. Dark spheres represent polymer microparticles.

RESULTS AND DISCUSSIONS

Shrinking Particles

Enzymatic degradation of PCL particles with ~15 µm and ~30 µm in radius was performed using enzyme at 150 LU g^{-1} with a flow rate of 10 µL h^{-1}. These particles experience a constant reduction in size, following the shrinking particle pattern **(Fig 2. 3A and B)**. Particle conversion (r/R) was calculated over time by measuring the change in the particles' radius using image processing method.

Fitting r/R versus t with intermediate formation (*EP control)* mechanism predicted the τ at ~140 min for 15 µm particles and ~470 min for 30 µm particles (**Fig S2. 5** and **Table S2. 3**). These values were higher than the experimental time observations, therefore the *EP control* cannot be the RDS (**Fig 2. 3A and B**). The bond cleavage (*RXN control*) mechanism predicts τ equal to be 91 mins for ~15 µm particles and 275 mins for ~30 µm particles (**Fig 2. 3C** and **D**). In our experimental observations particles were found to be completely degraded within similar time frames, thus indicating that this RDS model was a good fit **(Fig 2. 3** and **Movie S1)**. Further, if the *RXN control* mechanism is the RDS, because τ is a function of A_0, the normalized

characteristic time (τ/A_0) should remain constant for particles with a difference in radius at any specific enzyme concentration [E]. Our calculations indicate that the value of (τ/A_0) for ~30 μm particles and ~15 μm particles is not significantly different ($p < 0.05$) (**Table 2.1**). The close match of the experimentally observed and the calculated (τ/A_0) indicates that enzymatic particle degradation is governed by *RXN control* mechanism.

Using the identified RDS, the rate constant *k'* and *n* is calculated by performing similar experiments on ~15 μm particles using the enzyme at 1500 and 150 LU g^{-1} concentrations (**Fig. S2. 6**). The degradation kinetics of PCL were found to be independent of enzyme concentration from 15 kLU g^{-1} to 150 LU g^{-1}, indicating that the enzymatic degradation of PCL particles is a zero-order reaction governed by the *RXN control* mechanism (**Table 2.1**). The rate of degradation of PCL particles equation thus transforms to $(\frac{r}{R})^2 = 1 - \frac{k'}{A_0}t$, where k' = 34.6 ± 2.5 $\mu m^2\ min^{-1}$ using **Eq. 20**.

Table 2. 1: Detailed results for enzymatic degradation of PCL microparticles assuming RXN control degradation mechanism.

[E]	**15 kLU g^{-1}**	**1.5 kLU g^{-1}**	**150 LU g^{-1}**	**150 LU g^{-1}**
Radius (μm)	15.9 ± 1.1	15.6 ± 0.6	16.2 ± 1.2	28.8 ± 1.0
τ (min)*	95.3 ± 1.7	92.5 ± 1.3	90.9 ± 1.1	275.2 ± 2.6
$\frac{\tau}{A_0} \times 10^2$ (min μm^{-2})	3.06 ± 0.37[a]	3.04 ± 0.32[a]	2.78 ± 0.38[a]	2.65 ± 0.2[a]
k' (μm min^{-1})	33.0 ± 4.0[b]	33.1 ± 3.5[b]	36.3 ± 4.9[b]	37.8 ± 2.2[b]

* Predicted by the model assuming *RXN control* mechanism as the RDS.
Different letters in each row indicate significant statistical difference by one-way ANOVA Tukey's test ($p<0.05$). Values were given as mean±SD.

Unlike our findings, a previously developed model for enzymatic degradation of PCL and other polyester microparticles suggests a linear relationship between conversion and time (r/R vs. t), even though their experimental results did not comply with that model especially, at higher

conversion rates [(r/R) < 0.4].[1] This is a clear indication of the advantages of our SPM-SCM model over inaccuracies in the previously reported model as it accurately predicts the mechanism of degradation, characteristic time, and conversion rate at any given time.

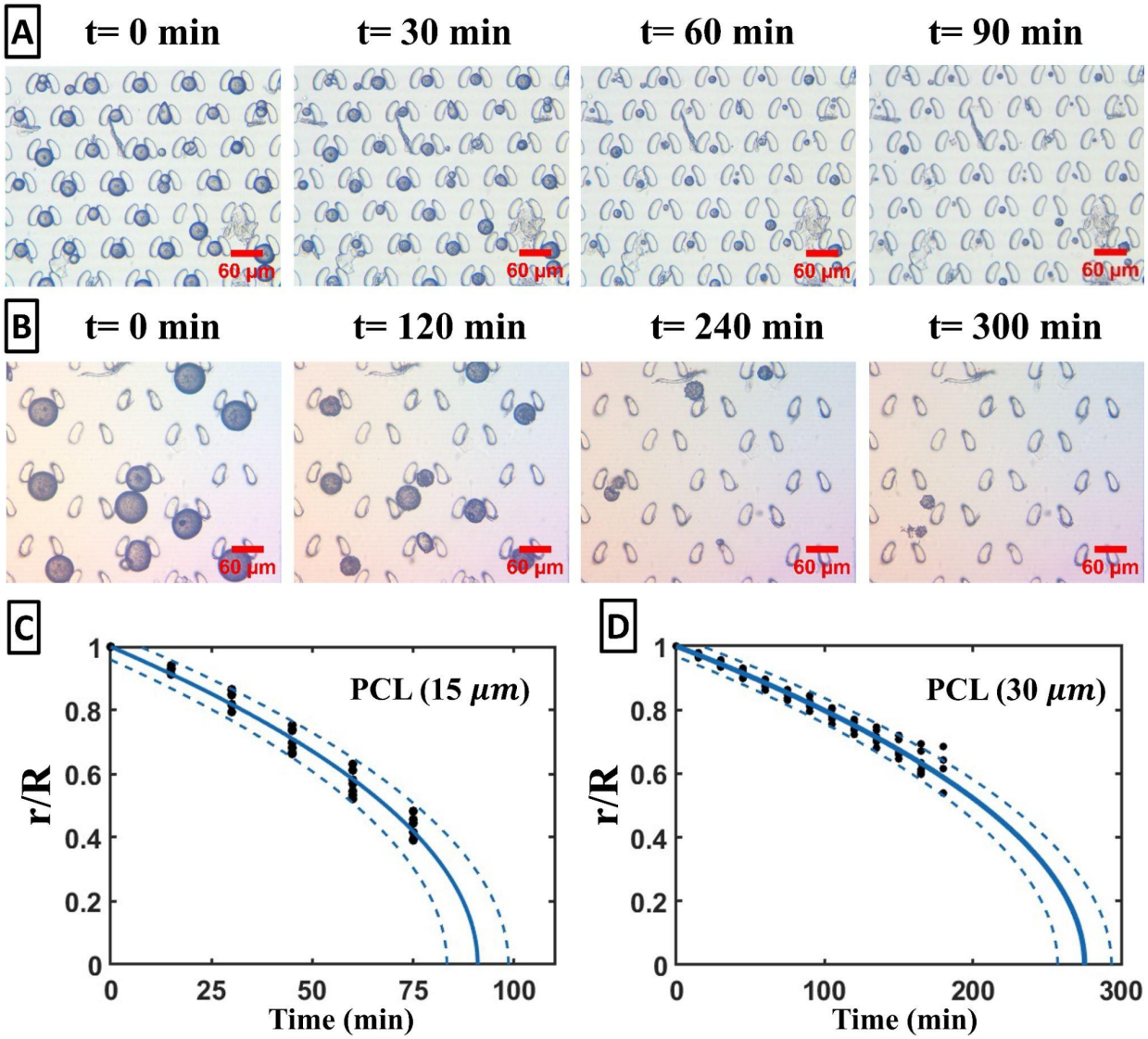

Figure 2. 3: Time lapse of enzymatic degradation of PCL particles with **A)** ~15 µm and **B)** ~30 µm in radius using 150 LU g^{-1} enzyme solution (scale bar = 60 µm). Conversion-time data of enzymatic degradation of PCL micro particles (black dots) with **C)** ~15 µm and **D)** ~30 µm and fitted curves of RXN control mechanism (blue line). Dashed lines indicate 95% confidence bands.

Core-shrinking Particles

PBAT is an aromatic aliphatic polyester containing hard and soft segments. These particles, upon enzymatic degradation, do not experience shrinkage, rather, their appearance transforms from opaque to transparent.[4] The size of the unreacted core shrinks as the degradation proceeds which makes this polymer a suitable candidate on which to apply the shrinking-core model.

To find the RDS, PBAT particles with ~20 μm radii were subjected to degradation using 15 kLU g^{-1} enzyme solution **(Fig 2. 4A** and **Video S2)**. The appearance of the particles as they shifted from opaque particles to transparent particles was monitored over time. To quantify the changes, the average gray value of the particle, at any given time, was measured by image processing tools and normalized to its maximum (background) and the minimum (darkest). Thus, the darkness was calculated as following:

$$relative\ darkness = 1 - \frac{particles\ gray\ value - minimum\ particle\ gray\ value}{background\ gray\ value - minimum\ particle\ gray\ value} \qquad (28)$$

Once the particles' darkness reaches a minimum (maximum transparency), the degradation was considered completed and τ was found to be ~68 h. We observed that the particles get slightly darker (~10%) at the initial stages of degradation **(Fig 2. 4C)**. We attribute this to the degradation of the amorphous regions on the surface of the particle, which led to an initial increase in the ratio of crystalline regions to amorphous regions of the substrate which caused the particles to diffract light and appear darker.[5] Nevertheless, monitoring the change in particle darkness fails to provide accurate time-resolved information for the shrinkage of the core (r/R vs. t).

According to SCM model, water (and enzyme) molecules cannot penetrate through the unreacted core, and the reactions take place solely on its surface. To evaluate this assumption, PBAT microparticles were immobilized in the microfluidic channel and treated with a buffer solution containing fluorescein dye (no enzyme added). No change in the fluorescence properties of the particles was observed after 48 h, confirming the impermeability of the particles (**Fig S2. 7**).

The ash layer, however, is assumed to be permeable to water and other solutes in the solution. Thus, fluorescence imaging can be used to distinguish the unreacted core from the ash layer. The difference in fluorescence between the ash layer and unreacted core allowed for a more accurate measurement of the radius of the ash layer compared to the unreacted core and confirmed the shrinking core degradation mechanism at the initial stage of degradation (r/R>0.6) (**Fig 2. S8**). After that, the difference in contrast between the ash and unreacted core decreases to the point at which the radius of unreacted core becomes immeasurable.

Plotting conversion (r/R) versus time as extrapolated from the results of fluorescent imaging with the proposed RDS models suggests that the enzymatic degradation of PBAT particles is governed by the *RXN control* mechanism (**Table S2. 4 and Fig S2. 9**). This mechanism most accurately predicts the characteristic time, τ, which for core-shrinking particles is equal to the time required for particles' darkness to reach a minimum **(Fig 2. 4C and Table S2. 4)**. In order to confirm this, τ was calculated for ~15 μm particles under similar test conditions and was found to be ~33 h **(Fig 2. 4B and C)**. Because the normalized characteristic times ($\frac{\tau}{A_0}$) for ~20 μm particles and ~15 μm particles were not significantly different ($p < 0.05$), the *RXN control* mechanism is found as the RDS (**Table 2. 2**).

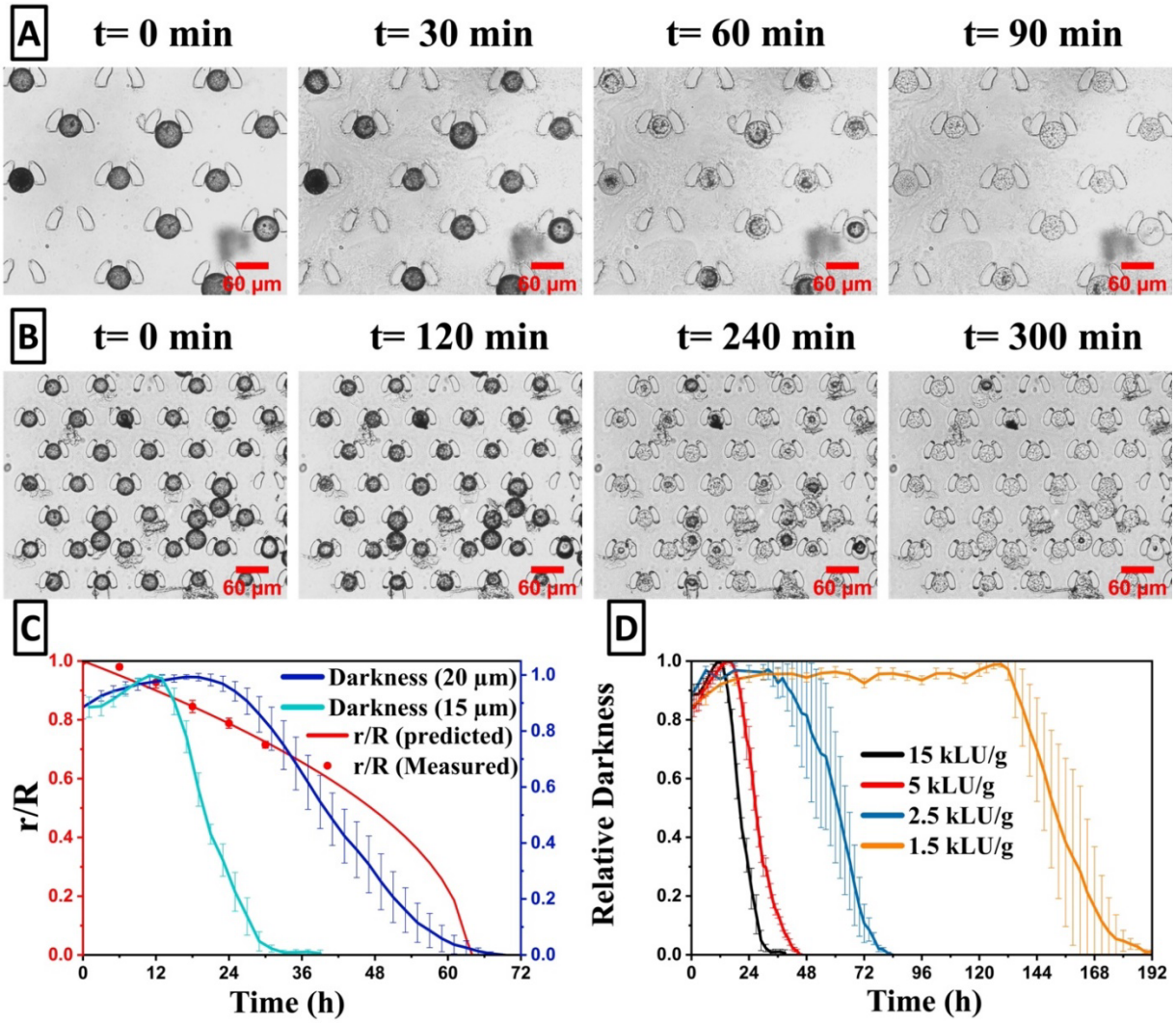

Figure 2. 4: Time lapse of enzymatic degradation of PBAT microparticles with **A)** ~20 µm and **B)** ~15 µm in radius using enzyme at 15 kLU g^{-1}. Scale bar is 60 µm. **C)** relative darkness, measured and predicted conversion rate (r/R) for PBAT particles with ~15 µm and ~20 µm in radius assuming RXN control mechanism as the RDS. **D)** change in the relative darkness of PBAT particles with ~15 µm in radius using enzyme at different concentrations.

The degradation of 15 µm particles was further investigated using different concentrations of enzyme to calculate *k'* and *n* (**Table 2**). The change in particle darkness over time was monitored to measure the τ **(Fig 2. 4D)**. Then by fitting $(\frac{\tau}{A_0}\ vs.\ [E])$ using equation

(20), we found that the overall degradation rate of PBAT that was first-order ($n = 0.98 \pm 0.04$) **(Fig 2. 5)**. The overall equation for the rate of degradation transforms to $\left(\frac{r}{R}\right)^2 = 1 - \frac{k'}{A_0}[E]t$ were $k' = (1.31 \pm 0.02) \times 10^{-2} \left[\frac{g.\ \mu m^2}{kLU.\ h}\right]$.

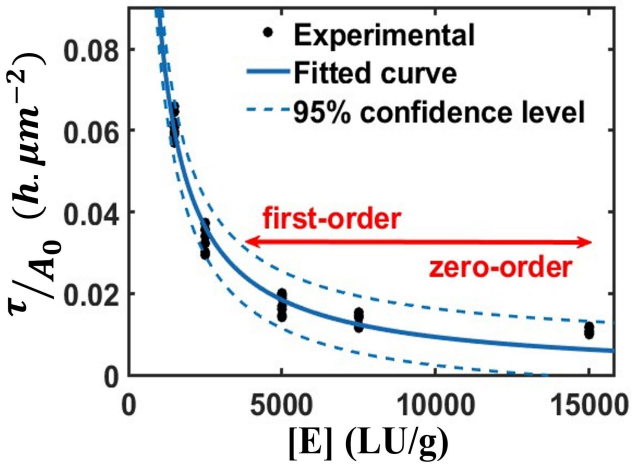

Figure 2. 5: Calculated τ/A_0 vs. [E] for PBAT microparticles with ~15 µm in radius and fitted curve assuming $\frac{\tau}{A_0} = \frac{1}{k'[E]^n}$

Table 2. 2: Detailed results for enzymatic degradation of PBAT microparticles

[E]	15 kLU g^{-1}	15 kLU g^{-1}	7.5 kLU g^{-1}	5 kLU g^{-1}	2.5 kLU g^{-1}	1.5 kLU g^{-1}
Radius (µm)	22.1±1.5	15.6 ± 0.7	16.5 ± 0.8	14.5 ± 1.0	14.0 ± .9	15.4±0.4
τ (h)	64.7±1.9	33.3 ± 1.9	45.0 ± 2.7	45.7 ± 0.4	83.4 ± 3.9	181.7 ± 8.6
$\frac{\tau}{A_0} \times 10^2$ (h µm^{-2})	1.06 ±0.14^a	1.08 ±0.07^a	1.32 ±0.15^b	1.75 ±0.23^c	3.37 ±0.32^d	6.13 ± 0.3^e

Different letters in each row indicate significant statistical difference by one-way ANOVA Tukey's test ($p<0.05$). Values were given as mean ± SD.

Experimental results indicate that enzyme concentrations above 7.5 kLU g^{-1} only mildly affect τ, therefore, the degradation kinetics are zero-order under such conditions. However, when the enzyme concentration is lower than 7.5 kLU g^{-1} the degradation kinetics become first order **(Fig 2. 5).** Similarly, the classic Michaelis-Menten model suggests zero-order reaction at high

[E] (lower substrate concentration) and first order at low [E] (higher substrate concentration). These findings are consistent with previous reports in which zero-order and first order kinetics were attributed to "enzyme excess" and "surface excess" conditions, respectively.[1]

PBSeT is another aromatic aliphatic co-polymer which contains longer aliphatic soft segments (sebacate) compared to PBAT (adipate). The degradation of PBSeT microparticles with ~15 μm radii exhibited a similar pattern as PBAT particles using 1.5 kLU g^{-1} enzyme solution. The characteristic time was found to be ~95 h, which is almost half the characteristic time calculated for PBAT under these conditions (**Fig S2. 11 and S2. 13**). Previous reports claimed that the presence of longer aliphatic chains, or a lower content of aromatic segments, contributed to an increase in enzyme activity due to the lower ability of PBSeT to form hard segment microdomains compared with PBAT.[39] Others have reported that the effect of polymer's chemical structure on enzymatic hydrolysis outweighs the effect of the substrate's crystallinity.[1] Our results support the latter hypothesis considering our observation that PBSeT degraded almost twice as fast as PBAT, but PBSeT has higher crystallinity (26%) than PBAT (12%).

To extend this, enzymatic degradation of PBS microparticles was studied. PBS possesses a fully aliphatic backbone with shorter soft segments (succinate) compared to PBAT but with higher crystallinity (43%). PBS particles fully degrade in ~70 h using only 150 LU g^{-1} (**Fig S2. 12-13**). Comparing the degradation rates and the degree of crystallinity of PBAT, PBSeT, and PBS, we believe that the chemical structure of the substrate has a more profound effect on the kinetics of degradation, rather than their extent of crystallinity. However, to have a solid conclusion on the effect of substrate's chemical structure and crystallinity on the degradation

kinetics, a more systematic and comprehensive study is required, which is outside the scope of this report.

CONCLUSION

Generalized Shrinking Particle (SPM) and Shrinking Core (SCM) models were developed to describe the steps involved in the enzymatic degradation kinetics of polymers with varying chemical compositions and crystallinity. Enzymatic degradation was performed on a microfluidic device to collect time-resolved data regarding the degradation of PCL and PBAT microparticles via image processing methods. PCL particles followed the SPM model, while the degradation PBAT, PBSeT, and PBS microparticles followed the SCM model.

The degradation of PCL microparticles was explained by plotting their time-conversion data, derived from monitoring the change in their size, with all the possible mechanisms of degradation. The bond cleavage (*RXN control*) mechanism accurately predicted the time required for full degradation of PCL with zero-order kinetics.

By monitoring PBAT particles during degradation we observed changes in their darkness and full degradation was determined when the particles were completely transparent. Fluorescent imaging successfully distinguished the unreacted core of the PBAT microparticles from the ash layer. This enabled measurement of the size of the unreacted core throughout the initial stages of degradation. The RDS for the degradation of PBAT microparticles was found by fitting experimental degradation time from fluorescent imaging to the possible RDS equations proposed for the SCM. Considering the predicted full degradation time, it was found that PBAT degradation is similar to PCL degradation and follows the bond cleavage (*RXN Control*) mechanism with first-order kinetics.

Degradation of PBSeT and PBS microparticles were also briefly studied. No direct correlation between the crystallinity of substrates and degradation kinetics was found and chemical structure seems to dominate these phenomena.

The combination of a microfluidic platform, coupled with the proposed models can be used to shed light on enzymatic degradation mechanisms. We demonstrated the robustness and accuracy of the described model integrated with a microfluidic platform that can be used as a standard method to correlate and elucidate the kinetic parameters of the degradation of water-insoluble polymers.

SUPPORTING INFORMATION

Materials

Polybutylene adipate-co-terephthalate (PBAT), Polybutylene Sebacate-co-terephthalate (PBSeT), and Polybutylene succinate (PBS) were provided by BASF (Tarrytown, NY, USA). Novozyme 51032 cutinase enzyme from *Humicola insolens* (15000 Lipase Units g^{-1} (15 kLU g^{-1})) was purchased from Strem Chemicals Inc. (Newburyport, MA, USA). Polycaprolactone (PCL, M_w ~80000 g/mol), Polyvinyl alcohol (PVA, Mowiol 10-98, M_w ~61000 g/mol), Fluorescein sodium, and Tween 80 were all purchased from Sigma-Aldrich (St. Louis, MO, USA). Sodium phosphate monobasic and sodium phosphate dibasic were purchased from Acros chemicals (Pittsburgh, PA, USA) to prepare 50 mM phosphate buffer at pH 7.6. This buffer was used to dilute enzyme stock solution. In all the steps, solvents used were reagent grade. In all the experiments, ultrapure MQ water was used.

Methods

The general method for using our microfluidic device to obtain experimental data regarding enzymatic degradation begins by priming the microfluidic channel with dilute Tween 80 in water (0.25 w/v%) to avoid particles aggregation and consequent clogging the microfluidic channel. Microparticles were dispersed in NaCl solution (~30 w/v%, matched to microparticle density), and containing 0.25 w/v% Tween 80. This mixture was then injected into the microfluidic channel. This process continued until a proper number of particles (10-20) were efficiently trapped and immobilized in the analytical region of the channel. Then, water was flushed through the channel to remove the salt and emulsifier. Finally, the enzyme solution (150 LU g^{-1}- 15 kLU g^{-1}) was introduced to the channel using a syringe pump at constant flow rate of

10 μL h^{-1} the approximate duration of experiments ranged from 2 to 200 h. For fluorescent imaging, the enzyme solution was spiked with fluorescein sodium salt (2 μg mL^{-1} final concentration). Particles were monitored and the change in their size and appearance was assessed during degradation to provide time-resolved particle conversion information via image processing methods. A detailed explanation regarding the fabrication of the microfluidic platform and additional methods can be found in the supporting information.

Summary of SPM-SCM Model

Table S2. 1: Summary of SPM-SCM model with associated RDSs.

RDS	SPM	SCM
Intermediate formation (EP control)	$t_{EP} = \tau_{EP}\left[1-\left(\frac{r}{R}\right)\right]$ $\tau_{EP} = \frac{\varepsilon\rho R}{K_1[E]^{\varepsilon}}$	$t_{EP} = \tau_{EP}\left[1-\left(\frac{r}{R}\right)\right]$ $\tau_{EP} = \frac{\varepsilon\rho R}{K_1[E]}$
Bond cleavage (RXN control)	$t_{RXN} = \tau_{RXN}\left[1-\left(\frac{r}{R}\right)^2\right]$ $\tau_{RXN} = \frac{A_0}{k'[E]^n}$	$t_{RXN} = \tau_{RXN}\left[1-\left(\frac{r}{R}\right)^2\right]$ $\tau_{RXN} = \frac{A_0}{k'[E]^n}$
Diffusion through the ash layer	N/A	$t_{\mathcal{D}} = \tau_{\mathcal{D}}\left[1-3\left(\frac{r}{R}\right)^2+2\left(\frac{r}{R}\right)^3\right]$ $\tau_{\mathcal{D}} = \frac{\varepsilon\rho R^2}{6\mathcal{D}[E]}$

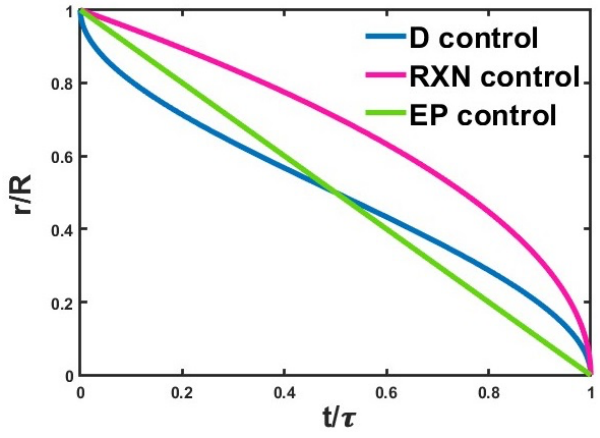

Figure S2. 1: Conversion-time curves with possible RDSs

Microparticle preparation:

The microparticles were prepared via conventional oil-in-water solvent extraction/evaporation method.[40] 100 mL of 4 w/w% PVA was used as the aqueous (continuous) phase. 50 mL of 10 w/v% polymer in chloroform (organic layer) was added dropwise to the aqueous layer held at 45 ºC while stirring by mechanical stirrer (IKA Eurostar 40 digital, Germany) at 500 rpm and 700 rpm for particles with radius >20 µm and >10 µm, respectively. After 5 h, particles were filtered by a nylon mesh filter with 15 µm mesh size (U-CMN-15, Component Supply Co., Tennessee, USA) or 38 µm mesh size (U-CMN-38) depending on the desired size range. Finally, particles were washed several times with water and dried via lyophilization. For SEM, samples were coated with gold/palladium using a sputter coater (Denton Desk V, NJ, USA). The coated samples were examined with an SEM (Zeiss Gemini 500, Jena, Germany). Objects were scanned with electron beam (1 keV) and visualized using a high-efficiency secondary-electron detector with a 30.0 µm aperture.

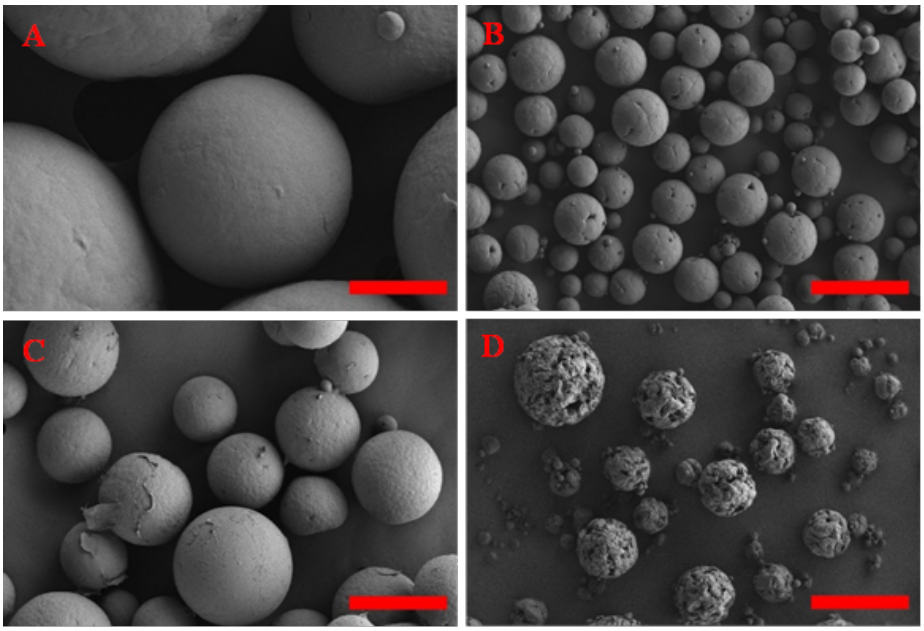

Figure S2. 2: SEM images of **A)** PCL, **B)** PBAT, **C)** PBSeT, **D)** PBS microparticles. Scale bar is 50 µm

Thermal Properties:

Differential Scanning Calorimetry experiments were performed using Q2500 TA Instruments (New Castle, DE, USA). Samples were heated from room temperature to 200 °C at 10 °C min^{-1} under nitrogen atmosphere. To measure the degree of crystallinity (X_c%) of PBSeT, Wide Angle X-ray Diffraction (WAXD) of its particles were analyzed using a Bruker D8 advanced eco with Cu k alpha X-ray source. Peaks found at 16.2°, 17.5°, 20.5°, 23.3°, and 24.5° correspond to crystal planes of PBSeT (**Fig S2. 3**) and similar to previously reported results.[41]

Table S2. 2: Thermal properties and molecular weight of microparticles

Material	PBAT	PBSeT	PBS	PCL
Xc % (particle)	9.1	26	41.7	30.6
Xc %	11.9	-	42.8	35.3
ΔH_{ref} (J g^{-1})	114 [42]	-	200 [43]	139.5 [44]

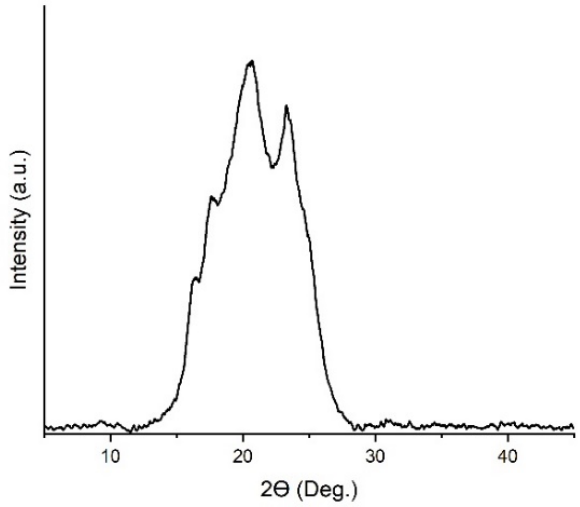

Figure S2. 3: WAXD diffractogram of PBSeT particles

Microfluidic Chip Design and Fabrication:

The channel contains two major regions. A separation region provides a well-dispersed flow of particles. Particles are trapped in the analytical region providing a uniform and statistically representative sample of physically immobilized particles. Enzymatic degradation of the particles was studied monitoring the particles in analytical region. All channels were fabricated via standard lithography methods. [45, 46] In summary, photoresist SU-8 2025 or SU-8 2050 (Microchem) was coated on a silicon wafer for channels with thickness of 35 µm and 50 µm, respectively. The master mold was prepared via UV-photolithography at 350 nm and removal of excess photoresist from wafers. Polydimethylsiloxane (PDMS) chip was prepared by mixing liquid PDMS and curing agent (Sylgard 184) at a 10:1 ratio. This mixture was then casted on the molds and cured for 3 hours. Cured PDMS chips were peeled off, punched, and bonded to glass slides via oxygen plasma bonding technique.

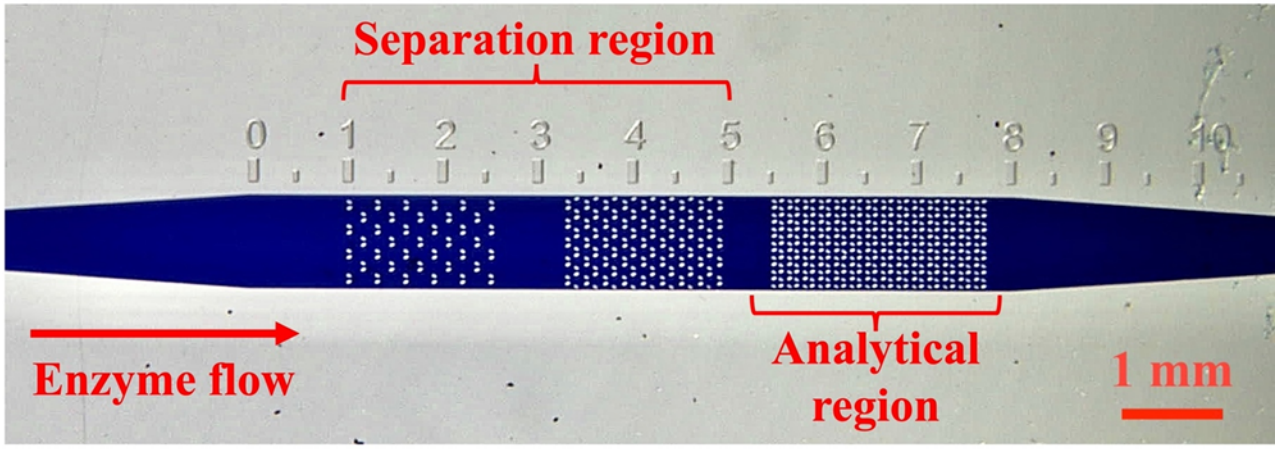

Figure S2. 4: Wide view of the microfluidic channel**.**

Image Processing and Modeling

Particle and unreacted-core size and darkness were measured over time using ImageJ software (NIH, Bethesda, MD. 1.53q). Mathematical modeling and curve fitting was performed by non-linear least-square regression method (Trust-region algorithm) using Matlab software (Mathworks, Inc. 2022a). OriginPro 2022.b. (OriginLab Corp., Northampton, MA.) was used to perform statistical analysis and prepare some of the figures.

Shrinking Particle:

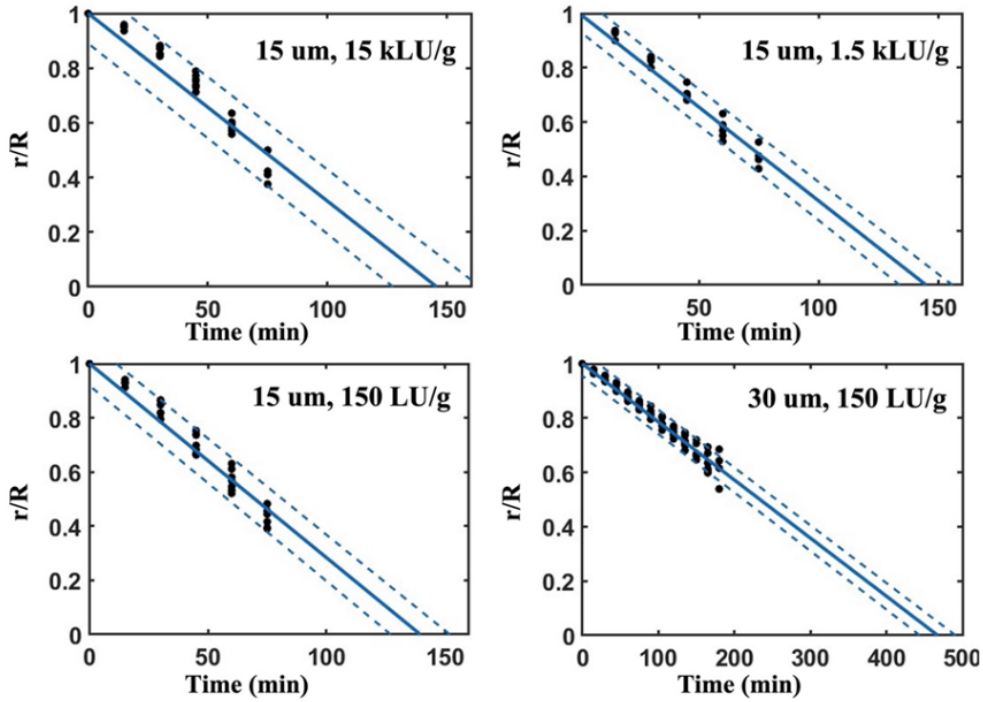

Figure S2. 5: Conversion-time data of enzymatic degradation of PCL micro particles (black dots) and fitted curves with EP control mechanism (blue line). Dashed lines indicate 95% prediction bonds.

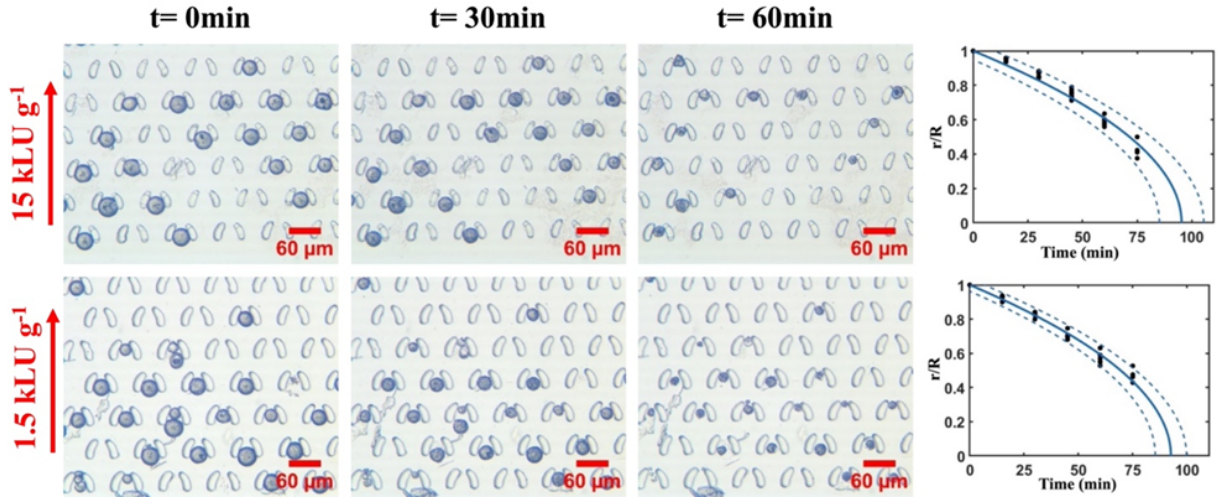

Figure S2. 6: Time lapse of enzymatic degradation of PCL microparticles with ~15 µm in radius using enzyme at 15 LU g^{-1} (top), and 1.5 kLU g^{-1} (bottom). Scale bar is 60 µm.

Table S2. 3: Detailed results of fitting the conversion-time of enzymatic degradation of PCL micro particles with RDS models

	τ (min)							
RDS	15 kLU g^{-1} (15.95 µm)	Fit (R^2)	1.5 kLU g^{-1} (15.6 µm)	Fit (R^2)	150 LU g^{-1} (16.2 µm)	Fit (R^2)	150 LU g^{-1} (28.8 µm)	Fit (R^2)
RXN control:	95.3 ± 1.7	0.9401	92.5 ± 1.3	0.9821	90.9 ± 1.1	0.9792	275.2 ± 2.6	0.9751
EP control:	145.6 ± 4.3	0.8698	145.0 ± 2.9	0.9604	139.6 ± 2.6	0.9623	467.1 ± 5.4	0.9641

Shrinking Core:

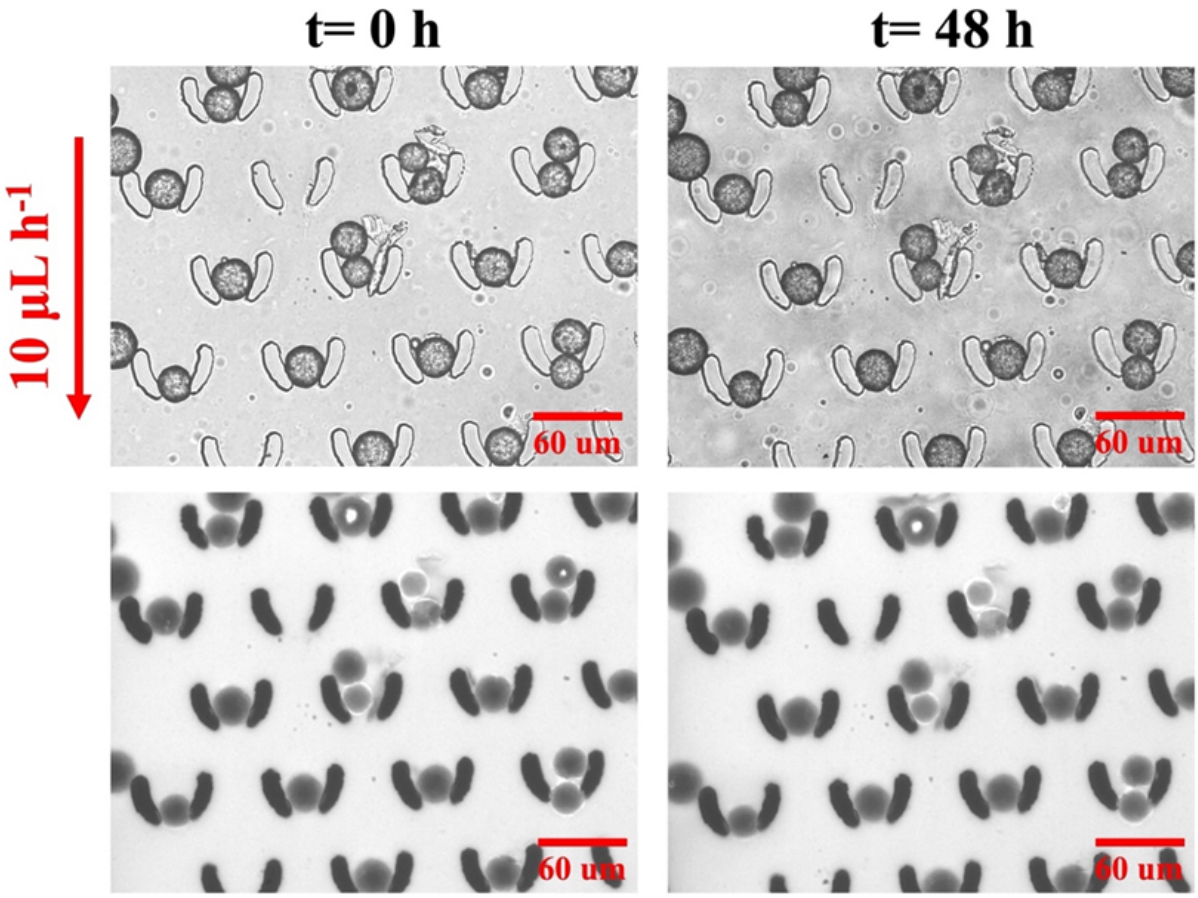

Figure S2. 7: Visible light (top) and fluorescent (bottom) images of PBAT particles (~15 µm) treated with buffer spiked with fluorescent dye.

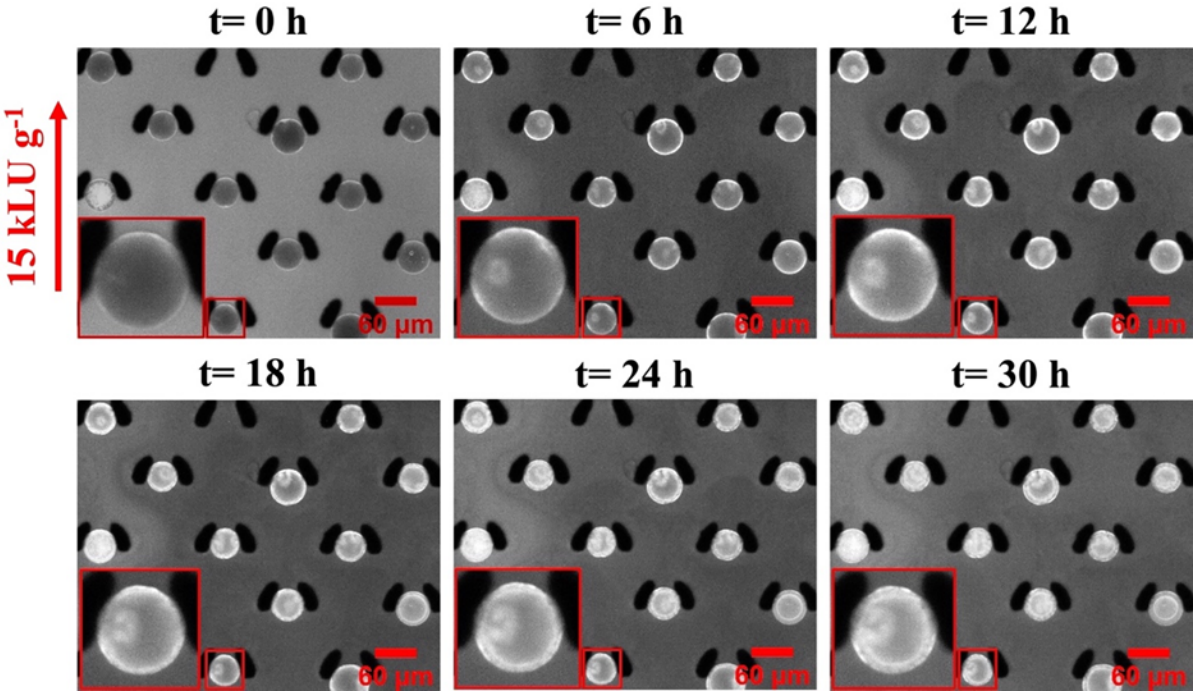

Figure S2. 8: Fluorescent images of PBAT particles (~20 µm) during enzymatic degradation.

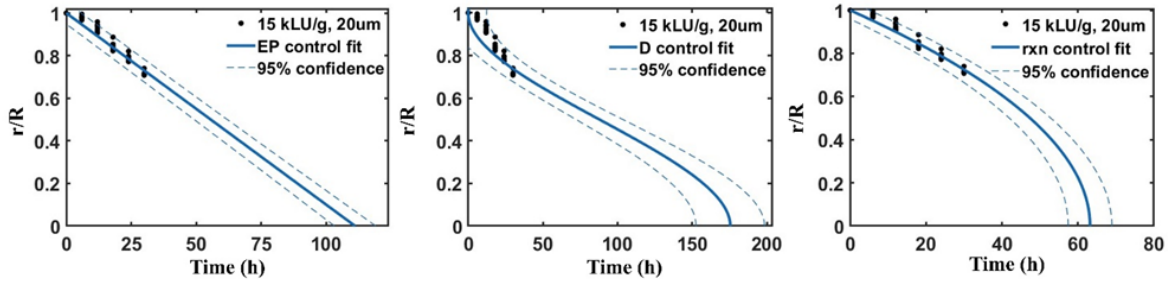

Figure S2. 9: Conversion-time data of enzymatic degradation of PBAT micro particles (black dots) and fitted curves with different mechanisms (blue line). Dashed lines indicate 95% prediction bonds.

Table S2. 4: Detailed results of modeling the conversion-time of enzymatic degradation of 20 µm PBAT micro particles at 15kLU g^{-1}

	RDS				
	RXN control:	EP control:	D control:	RXN + D control	EP + D control
τ (h)	63.2 ± 1.37	111.2 ± 2.75	175.4 ± 9.65	63.2 ± 1.37 + 4.077e-09	111.2 ± 2.75 + 4.708e-14
Fit (R^2)	0.9417	0.9246	0.6569	0.9417	0.9246

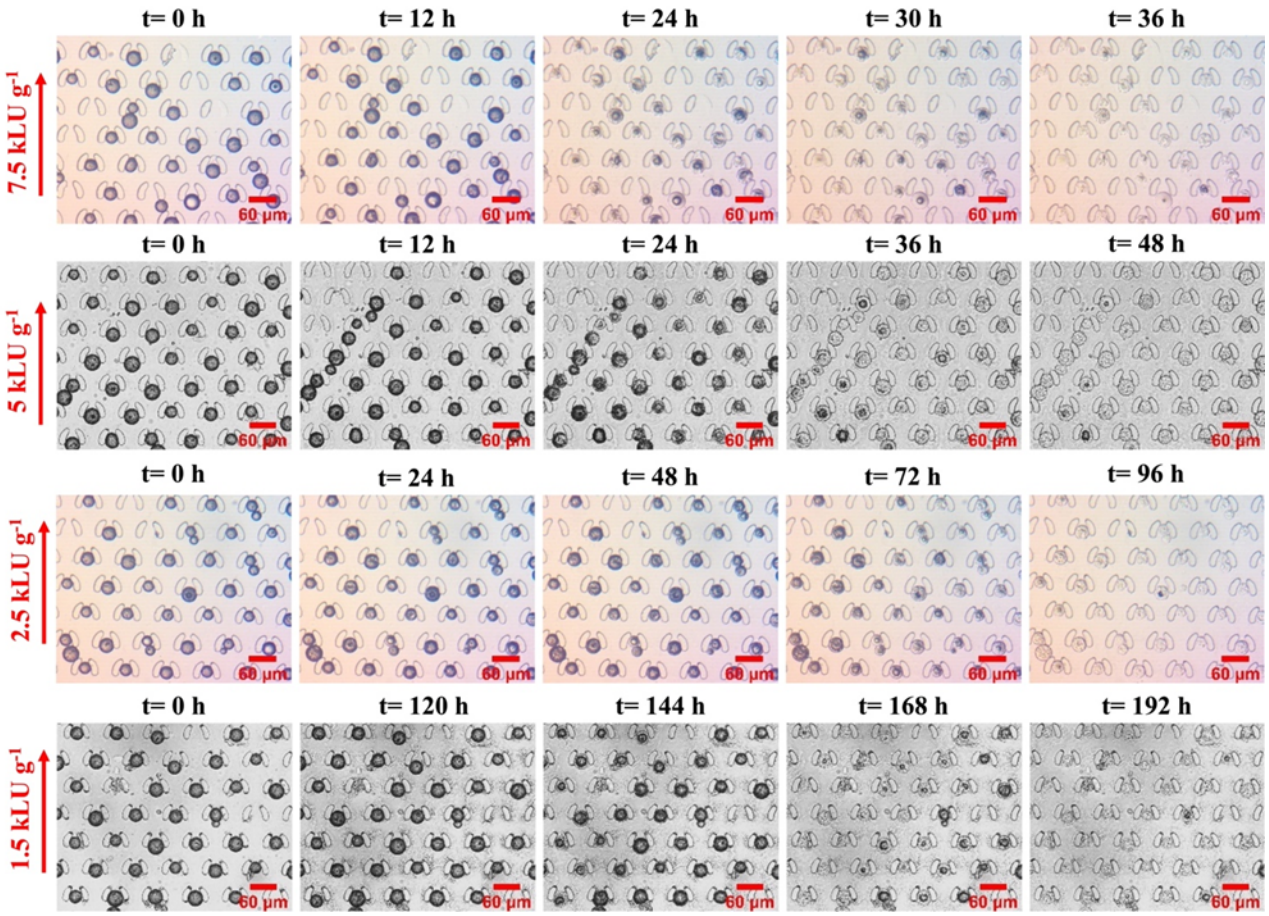

Figure S2. 10: Time lapse of enzymatic degradation of PBAT microparticles with ~15 µm in radius using enzyme at different concentrations. Scale bar is 60 µm.

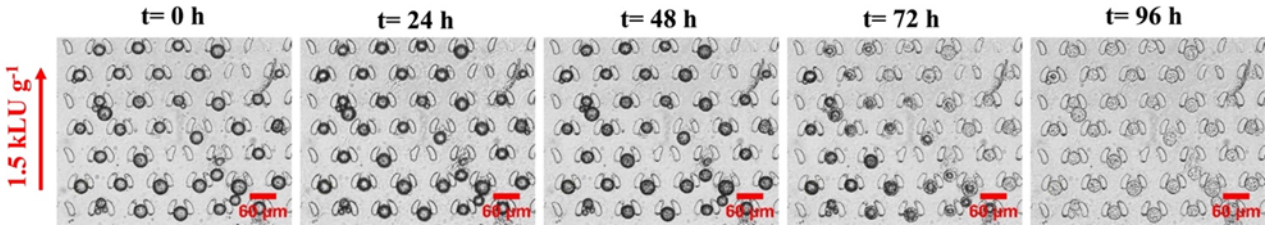

Figure S2. 11: Time lapse of enzymatic degradation of PBSeT microparticles with ~15 µm in radius using enzyme at 1.5 k LU g-1. Scale bar is 60 µm.

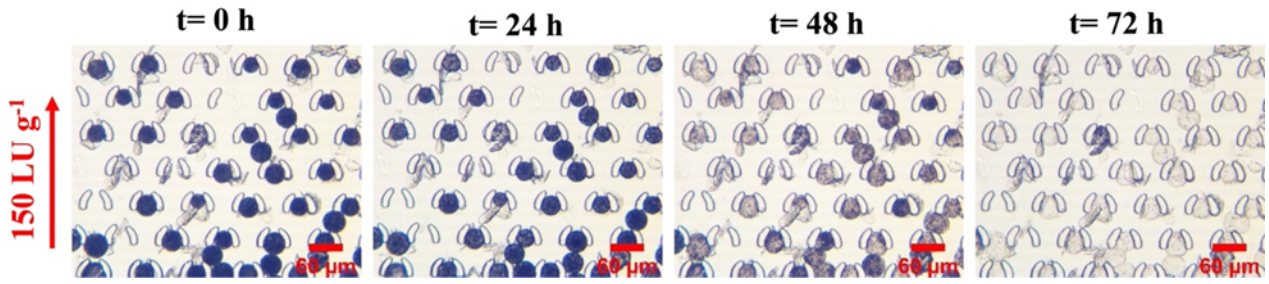

Figure S2. 12: Time lapse of enzymatic degradation of PBS microparticles with ~15 µm in radius using enzyme at 15 LU g-1. Scale bar is 60 µm.

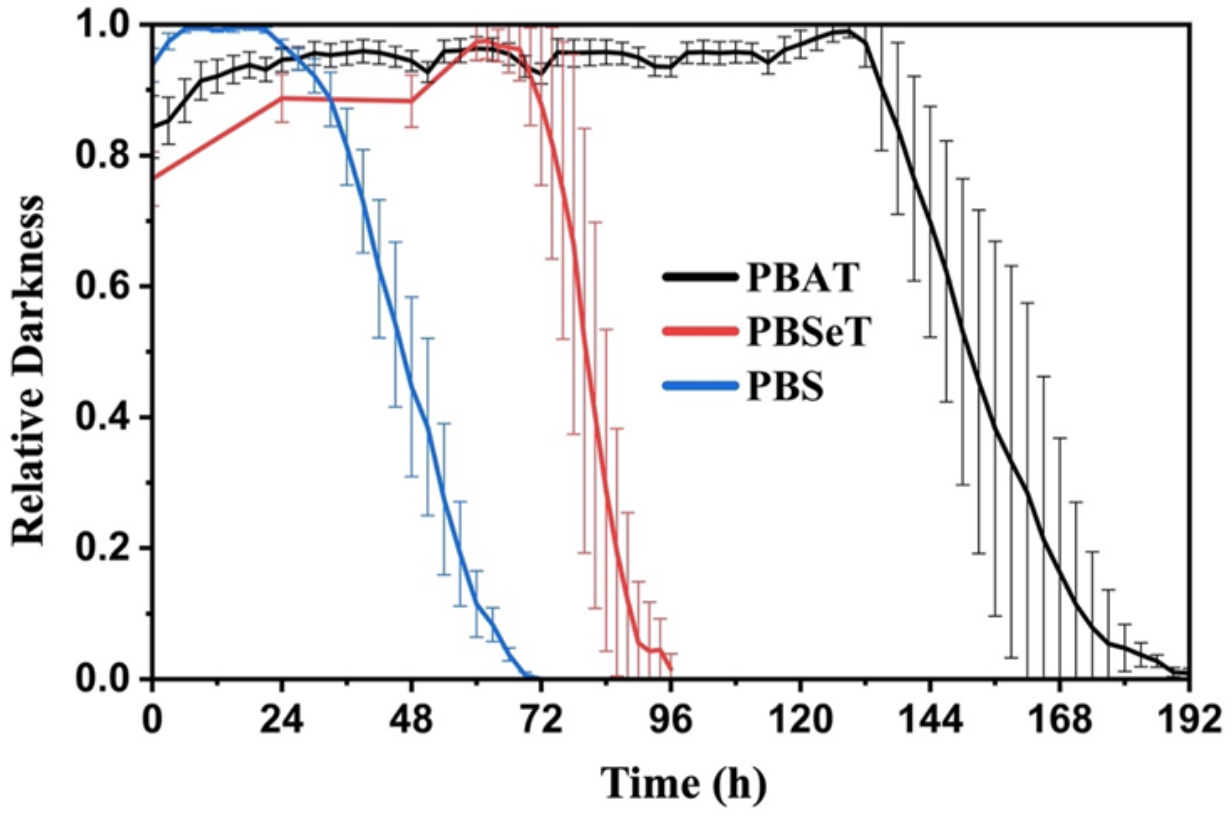

Figure S2. 13: Change in the particles' darkness over time during degradation using enzyme at 1.5 k LU g-1 (PBAT and PBSeT) and 150 LU g^{-1} (PBS)

REFERENCES

(1) Herzog, K.; Müller, R.-J.; Deckwer, W.-D. Mechanism and Kinetics of the Enzymatic Hydrolysis of Polyester Nanoparticles by Lipases. *Polymer degradation and stability* **2006**, *91* (10), 2486–2498.

(2) Rahmouni, M.; Chouinard, F.; Nekka, F.; Lenaerts, V.; Leroux, J. C. Enzymatic Degradation of Cross-Linked High Amylose Starch Tablets and Its Effect on in Vitro Release of Sodium Diclofenac. *European journal of pharmaceutics and biopharmaceutics* **2001**, *51* (3), 191–198.

(3) Liu, L.; Li, S.; Garreau, H.; Vert, M. Selective Enzymatic Degradations of Poly (L-Lactide) and Poly (ε-Caprolactone) Blend Films. *Biomacromolecules* **2000**, *1* (3), 350–359.

(4) Davachi, S. M.; Mokhtare, A.; Torabi, H.; Enayati, M.; Deisenroth, T.; Van Pho, T.; Qu, L.; Tücking, K.-S.; Abbaspourrad, A. Screening the Degradation of Polymer Microparticles on a Chip. *ACS Omega* **2022**.

(5) Li, S. Hydrolytic Degradation Characteristics of Aliphatic Polyesters Derived from Lactic and Glycolic Acids. *Journal of Biomedical Materials Research: An Official Journal of The Society for Biomaterials, The Japanese Society for Biomaterials, and The Australian Society for Biomaterials* **1999**, *48* (3), 342–353.

(6) Schusser, S.; Krischer, M.; Bäcker, M.; Poghossian, A.; Wagner, P.; Schöning, M. J. Monitoring of the Enzymatically Catalyzed Degradation of Biodegradable Polymers by Means of Capacitive Field-Effect Sensors. *Analytical chemistry* **2015**, *87* (13), 6607–6613.

(7) Leinhos, M.; Schusser, S.; Bachmann, B.; Bäcker, M.; Poghossian, A.; Schöning, M. J. Micromachined Multi-parameter Sensor Chip for the Control of Polymer-degradation Medium. *physica status solidi (a)* **2014**, *211* (6), 1346–1351.

(8) Nghe, P.; Tabeling, P.; Ajdari, A. Flow-Induced Polymer Degradation Probed by a High Throughput Microfluidic Set-Up. *Journal of Non-Newtonian Fluid Mechanics* **2010**, *165* (7–8), 313–322.

(9) Grayson, A. C. R.; Choi, I. S.; Tyler, B. M.; Wang, P. P.; Brem, H.; Cima, M. J.; Langer, R. Multi-Pulse Drug Delivery from a Resorbable Polymeric Microchip Device. *Nature materials* **2003**, *2* (11), 767–772.

(10) Intra, J.; Glasgow, J. M.; Mai, H. Q.; Salem, A. K. Pulsatile Release of Biomolecules from Polydimethylsiloxane (PDMS) Chips with Hydrolytically Degradable Seals. *Journal of Controlled Release* **2008**, *127* (3), 280–287.

(11) Wouters, B.; Pirok, B. W.; Soulis, D.; Perticarini, R. C. G.; Fokker, S.; van den Hurk, R. S.; Skolimowski, M.; Peters, R. A.; Schoenmakers, P. J. On-Line Microfluidic Immobilized-Enzyme Reactors: A New Tool for Characterizing Synthetic Polymers. *Analytica chimica acta* **2019**, *1053*, 62–69.

(12) Scandola, M.; Focarete, M. L.; Frisoni, G. Simple Kinetic Model for the Heterogeneous Enzymatic Hydrolysis of Natural Poly (3-Hydroxybutyrate). *Macromolecules* **1998**, *31* (12), 3846–3851.

(13) Polyák, P.; Dohovits, E.; Nagy, G. N.; Vértessy, B. G.; Vörös, G.; Pukánszky, B. Enzymatic Degradation of Poly-[(R)-3-Hydroxybutyrate]: Mechanism, Kinetics, Consequences. *International journal of biological macromolecules* **2018**, *112*, 156–162.

(14) Ronkvist, Å. M.; Xie, W.; Lu, W.; Gross, R. A. Cutinase-Catalyzed Hydrolysis of Poly (Ethylene Terephthalate). *Macromolecules* **2009**, *42* (14), 5128–5138.

(15) Mata-Perez, F.; Perez-Benito, J. F. The Kinetic Rate Law for Autocatalytic Reactions. *Journal of Chemical Education* **1987**, *64* (11), 925.

(16) Xu, Y.; Sen, S.; Wu, Q.; Zhong, X.; Ewoldt, R. H.; Zimmerman, S. C. Base-Triggered Self-Amplifying Degradable Polyurethanes with the Ability to Translate Local Stimulation to Continuous Long-Range Degradation. *Chemical science* **2020**, *11* (12), 3326–3331.

(17) Osada, K.; Akahori, R.; Suzuki, Y.; Matsumoto, A. Controlled Deprotection of Poly (2-(Tert-Butoxycarbonyloxy) Ethyl Methacrylate) Using p-Toluenesulfonic Esters as Thermally Latent Acid Catalysts. *Polymer Degradation and Stability* **2022**, 110127.

(18) Miller, K. A.; Morado, E. G.; Samanta, S. R.; Walker, B. A.; Nelson, A. Z.; Sen, S.; Tran, D. T.; Whitaker, D. J.; Ewoldt, R. H.; Braun, P. V. Acid-Triggered, Acid-Generating, and Self-Amplifying Degradable Polymers. *Journal of the American Chemical Society* **2019**, *141* (7), 2838–2842.

(19) Ranzi, E.; Corbetta, M.; Manenti, F.; Pierucci, S. Kinetic Modeling of the Thermal Degradation and Combustion of Biomass. *Chemical Engineering Science* **2014**, *110*, 2–12.

(20) Salmi, T.; Grénman, H.; Wärnå, J.; Murzin, D. Y. Revisiting Shrinking Particle and Product Layer Models for Fluid–Solid Reactions–From Ideal Surfaces to Real Surfaces. *Chemical Engineering and Processing: Process Intensification* **2011**, *50* (10), 1076–1084.

(21) Homma, S.; Ogata, S.; Koga, J.; Matsumoto, S. Gas–Solid Reaction Model for a Shrinking Spherical Particle with Unreacted Shrinking Core. *Chemical Engineering Science* **2005**, *60* (18), 4971–4980.

(22) Gou, H.; Zhang, G.; Hu, X.; Chou, K. Kinetic Study on Carbothermic Reduction of Ilmenite with Activated Carbon. *Transactions of Nonferrous Metals Society of China* **2017**, *27* (8), 1856–1861.

(23) Li, D.; Wang, Y.; Li, Z. Limestone Calcination Kinetics in Microfluidized Bed Thermogravimetric Analysis (MFB-TGA) for Calcium Looping. *Catalysts* **2022**, *12* (12), 1661.

(24) da Rocha, D.; Paetzold, E.; Kanswohl, N. The Shrinking Core Model Applied on Anaerobic Digestion. *Chemical Engineering and Processing: Process Intensification* **2013**, *70*, 294–300.

(25) Hashemi, S. M.; Sedghkerdar, M. H.; Mahinpey, N. Calcium Looping Carbon Capture: Progress and Prospects. *The Canadian Journal of Chemical Engineering* **2022**, *100* (9), 2140–2171.

(26) Abedsoltan, H.; Coleman, M. R. Aryl Sulfonic Acid Catalysts: Effect of Pendant Group Structure on Activity in Hydrolysis of Polyethylene Terephthalate. *Journal of Applied Polymer Science* **2022**, *139* (27), e52451.

(27) Abedsoltan, H.; Omodolor, I. S.; Alba-Rubio, A. C.; Coleman, M. R. Poly (4-Styrenesulfonic Acid): A Recoverable and Reusable Catalyst for Acid Hydrolysis of Polyethylene Terephthalate. *Polymer* **2021**, *222*, 123620.

(28) Biermann, L.; Quast, D.; Brepohl, E.; Eichert, C.; Scholl, S. Alkali Depolymerization of Poly (Ethylene Terephthalate) in a Quasi-solid-solid Kneading Reaction. *Chemical Engineering & Technology* **2021**, *44* (12), 2300–2308.

(29) López-Fonseca, R.; González-Velasco, J. R.; Gutiérrez-Ortiz, J. I. A Shrinking Core Model for the Alkaline Hydrolysis of PET Assisted by Tributylhexadecylphosphonium Bromide. *Chemical Engineering Journal* **2009**, *146* (2), 287–294.

(30) Yoshioka, T.; Motoki, T.; Okuwaki, A. Kinetics of Hydrolysis of Poly (Ethylene Terephthalate) Powder in Sulfuric Acid by a Modified Shrinking-Core Model. *Industrial & engineering chemistry research* **2001**, *40* (1), 75–79.

(31) Yoshioka, T.; Okayama, N.; Okuwaki, A. Kinetics of Hydrolysis of PET Powder in Nitric Acid by a Modified Shrinking-Core Model. *Industrial & engineering chemistry research* **1998**, *37* (2), 336–340.

(32) de Castro, A. M.; Carniel, A.; Nicomedes Junior, J.; da Conceição Gomes, A.; Valoni, É. Screening of Commercial Enzymes for Poly (Ethylene Terephthalate)(PET) Hydrolysis and Synergy Studies on Different Substrate Sources. *Journal of Industrial Microbiology and Biotechnology* **2017**, *44* (6), 835–844.

(33) Göpferich, A. Mechanisms of Polymer Degradation and Erosion. *Biomaterials* **1996**, *17* (2), 103–114.

(34) Yang, R.; Rodriguez-Fernandez, M.; St. John, P. C.; Doyle, F. J. 8 - Systems Biology. In *Modelling Methodology for Physiology and Medicine (Second Edition)*; Carson, E., Cobelli, C., Eds.; Elsevier: Oxford, 2014; pp 159–187. https://doi.org/10.1016/B978-0-12-411557-6.00008-2.

(35) Rahimi, G.; Rastegar, S. O.; Chianeh, F. R.; Gu, T. Ultrasound-Assisted Leaching of Vanadium from Fly Ash Using Lemon Juice Organic Acids. *RSC advances* **2020**, *10* (3), 1685–1696.

(36) Thangaraj, B.; Solomon, P. R. Immobilization of Lipases–a Review. Part II: Carrier Materials. *ChemBioEng Reviews* **2019**, *6* (5), 167–194.

(37) Gitlesen, T.; Bauer, M.; Adlercreutz, P. Adsorption of Lipase on Polypropylene Powder. *Biochimica et Biophysica Acta (BBA)-Lipids and Lipid Metabolism* **1997**, *1345* (2), 188–196.

(38) Levenspiel, O. *Chemical Reaction Engineering*; John wiley & sons, 1998.

(39) Santerre, J. P.; Labow, R. S. The Effect of Hard Segment Size on the Hydrolytic Stability of Polyether-urea-urethanes When Exposed to Cholesterol Esterase. *Journal of biomedical materials research* **1997**, *36* (2), 223–232.

(40) Barbato, F.; La Rotonda, M. I.; Maglio, G.; Palumbo, R.; Quaglia, F. Biodegradable Microspheres of Novel Segmented Poly (Ether-Ester-Amide) s Based on Poly (ε-Caprolactone) for the Delivery of Bioactive Compounds. *Biomaterials* **2001**, *22* (11), 1371–1378.

(41) Kim, S. J.; Kwak, H. W.; Kwon, S.; Jang, H.; Park, S. Synthesis, Characterization and Properties of Biodegradable Poly (Butylene Sebacate-Co-Terephthalate). *Polymers* **2020**, *12* (10), 2389.

(42) Wang, H.; Wei, D.; Zheng, A.; Xiao, H. Soil Burial Biodegradation of Antimicrobial Biodegradable PBAT Films. *Polymer Degradation and Stability* **2015**, *116*, 14–22.

(43) Papageorgiou, G. Z.; Bikiaris, D. N. Crystallization and Melting Behavior of Three Biodegradable Poly (Alkylene Succinates). A Comparative Study. *Polymer* **2005**, *46* (26), 12081–12092.

(44) Lam, C. X.; Savalani, M. M.; Teoh, S.-H.; Hutmacher, D. W. Dynamics of in Vitro Polymer Degradation of Polycaprolactone-Based Scaffolds: Accelerated versus Simulated Physiological Conditions. *Biomedical materials* **2008**, *3* (3), 034108.

(45) Whitesides, G. M. Soft Lithography. *Annu. Rev. Mater. Sci.* **1998**, *28*, 153.

(46) Qin, D.; Xia, Y.; Whitesides, G. M. Soft Lithography for Micro-and Nanoscale Patterning. *Nature protocols* **2010**, *5* (3), 491.

Chapter 3: Novel Application

High-crystalline Polyhydroxy Butyrate systems for Controlled Release of Iron Micronutrient to Soil and Plants

INTRODUCTION

To meet the food demand for a predicted population of 9.6 billion (by 2050), agricultural productivity must improve more than ever. Although using fertilizers has the potential increase the production, their long-term and excessive use can negatively affect the soil quality and result in the pollution of land and marine ecosystems.[1] In this regard, design and application of controlled-release fertilizers has gained attraction in scientific societies. Most important micronutrients such as iron, zinc, and boron form nonbioavailable complexes upon their release in soil. As a result, traditional fertilizers are unable to efficiently address micronutrient delivery to crops and plants. In this regard, a controlled release of micronutrients in agricultural soil is of utmost importance to achieve a sustainable agriculture industry. Iron especially, in form of Fe^{2+} is a necessary micronutrient since it plays an important role in chlorophyll production and several other physiological processes in plants. Since most of the iron delivered by fertilizers in soil eventually become non-bioavailable, due to the oxidation, iron deficiency has become a major issue affecting the yield of crops. In this regard, protecting supplementary Fe^{2+} from oxidation and its controlled release is the subject of this study. This protection and controlled release mechanism needs to be biodegradable. Also, degradation byproducts must be non-toxic. Biodegradable polyhydroxy butyrate (PHB) is investigated for this application. The application of PHB in many industrial settings is limited due to its high crystallinity and low processibility. However, for this application, we take this generally accepted as negative characteristic in use to prepare biodegradable PHB nanocomposite powders for a controlled and prolonged release of iron to the soil.

PHB PRODUCTION

Plasmid Construction

PHB was produced by engineered *E.coli* JM109 harboring genes 3-ketothiolase (PhaA), acetoacetyl-CoA reductase (PhaB), PHA Synthase (PhaC) from *R. Eutropha* H16. The codon of phaCAB operon was optimized for *E. coli* and synthesized by Biomatik Corporation (Cambridge, Canada). phaCAB operon was then inserted in pBluscript II SK(+). *E.*coli JM109 competent cells were transformed with the plasmid using heat-shock method according to the manufacturer's protocol and plated on ampicillin containing Luria-Bertani (LB) agar media and incubated at 37°C. The full plasmid map and sequence are provided in supporting information.

Culture Conditions

A single colony of the cells were inoculated into 50 mL of LB media containing 100 μg/mL ampicillin and incubated for 18 h at 37°C. 5 mL on inoculum were then transferred to 2L flasks containing 500 mL of Terrific Broth (TB), 8 gr/L glycerol, and 100 μg/mL ampicillin. Cultures were incubated at 30°C with 250 RPM reciprocal shaking and after 4 h (OD= 550,) glucose (2% w/v) and Pantothenic acid (20 mM) were added, and incubation continued for 72 h.

Cell cultivation, PHB extraction and purification were performed according to our previous report. [2]

PHB Characterization

PHB molecular weight was analyzed by Gel Permeation Chromatography (GPC) device equipped with a Waters 410 differential refractive index detector and calibrated against polystyrene standards using THF as the mobile phase.

Table 3. 1: Culture condition and productivity of engineered *E.coli* for PHB production

Strain	Culture condition	CDW (g/L)	PHB (g/L)	PHB (%CDW)	Mn	PDI
E. coli BL 21	LB, 2% Xylose, 37°C, 72h	1.89 ± 0.06	0.026 ± 0.004	4.9 ±0.6	141 kDa	1.3
E. coli JM109	TB, 2% glucose, 2mM PA, 0.8% glycerol, 30°C, 72h	8.05 ± 0.3	3.65 ± 0.15	50.0 ± 2	1050 kDa	2.05

NANOFERTILIZER PRODUCTION

Iron Oxide Nanoparticles Fe_3O_4 (INP: 20-30 nm) purchased from SkySpring Nanomaterials (Houston, TX) was dispersed in chloroform (10 mg/mL) by sonication for 10 m using Sonics Vibra Cell VC750 Ultrasonic Homogenizer with Probe model CV334. To this suspension, PHB solution in chloroform (2 % w/v) was added dropwise while sonicating. Sonication continued for another 30 m and the final solution was transferred to levelled glass molds. After solvent removal, PHB-Iron nanocomposites (PHB-INP) were detached from the molds and hot pressed for 30 s to prepare PHB-Iron nanocomposite films at 190°C and pressure of 5 MPa.

Films were used for degradation and morphological analysis. To prepare nano fertilizer (NF), films containing 30% w/w INP were powdered using a household coffee grinder to yield small granules with maximum 1 mm size.

NANOFERTILIZER CHARACTERIZAION

Thermal Properties

Thermal properties were measured by Differential Scanning Calorimetry (DSC) technique using a TA instrument DSC-2500 device under N_2 atmosphere. Samples were heated

to 200°C at a rate of 10°C/min and remained at this temperature for 5 min. They were then cooled down to -40°C to eliminate the thermal history. Finally, samples were heated to 200°C for the second heating cycle. Thermal properties and crystallization behavior were measured by Differential Scanning Calorimetry (DSC) technique using TA instruments DSC2500 device. Upon addition of INP, T_g of the nanocomposites have shifted to higher temperatures due to the restriction in movement of polymer chains caused by the INP. It was observed that the PHB (PHB 72) also shows higher T_g compared to PHB 48, which can be related to the higher molecular weight and more physical entanglements, due to the extended incubation of *E.coli* and consequently, longer polymerization period. The melting temperature of both PHB samples is relatively identical; however, by adding INP up to 10%, the melting temperature in nanocomposites has also shifted to a higher temperature since INP could act as a nucleating agent.[3, 4] The further decrease in INP contents higher than 10% could be due to the agglomeration of the nanoparticles and the creation of hotspots during the heating process. The agglomeration causes non-uniform heat transfer and decreases the melting temperature.[5] The crystallinity of the nanocomposites, as well as the ΔH_m , shows a decreasing trend, and upon the addition of 30% INP the values drastically decrease. The main possible reason could be the restrictions of the PHB chains' segmental motions caused by INP nanoparticles. In other words, the crystallinity decreases due to the PHB chains' failure to properly integrate into the developing crystalline lamella.[5] The width at half height (WHH) of the crystallization peaks, which indicates the crystallization rate, shows increasing values up to 10% INP content, which is a sign of good distribution of nanoparticles as they act as nucleating agents. However, due to the agglomeration, WHH values increased in higher contents.

Engineered *E.coli* JM109 using plasmid harboring phaCAB operon from *R. Eutropha* H16 was able to yield PHB with high molecular weight and consequently, higher degree of crystallinity (X_c=70%), which corroborates with previous studies.[7, 8] This higher crystallinity of the product compared with average molecular weight PHB (X_c=50%) confirms the optimization microbial process for both genetic engineering and growth condition. In addition to that, it allows the PHB matrix to contain more cargo (INP) without losing crystallinity. It is generally accepted that the higher crystallinity of the matrix results in a slower degradation rate. This is crucial for a controlled release system which release trigger mechanism is based on biodegradation.

Table 3. 2: Detailed thermal analysis of PHB and its nanocomposites

sample	PHB[a]	PHB[b]	PHB-I 5	PHB-I 10	PHB-I 20	PHB-I 30
INP content (w/w)	0	0	5	10	20	30
T_g (°C)	-3.8	1.6	3.5	4.7	5.9	6.9
T_m (°C)	175.0	174.9	179.6	179.9	176.0	169.7
ΔH_m (J/g)	73.7	96.1	73.6	73.5	73.4	44.5
WHH (°C)	14.8	17.9	16.4	16.2	18.8	20.3
X_c%[c]	50.5	65.8	50.4	50.3	50.2	30.5

[a] PHB yielded from growing engineered *E.coli* after 48 h
[b] PHB yielded from growing engineered *E.coli* after 72 h
[c] Considering melting enthalpy of 100% crystalline PHB 146 J/g [6]

Morphological Properties

To evaluate the well-dispersion of INP in PHB matrix, Scanning Electron Microscopic (SEM) images were taken from cross section of the film loaded with 30% INP. Samples were placed on a stub with conductive carbon tape, which were then coated with carbon using a sputter coater (Denton Desk V, NJ, USA). The coated samples were mounted on a 90° holder, and the edge of the film was examined with an SEM (Zeiss Gemini 500, Jena, Germany). SEM imaging with energy-dispersive X-ray spectroscopy (EDS) was used to observe the dispersion of

INP in the PHB nanocomposites. The nanoparticles contain “Fe” atoms (Red dots), and the good distribution of Fe atoms is a sign of proper dispersion of nanoparticles in the nanocomposites.

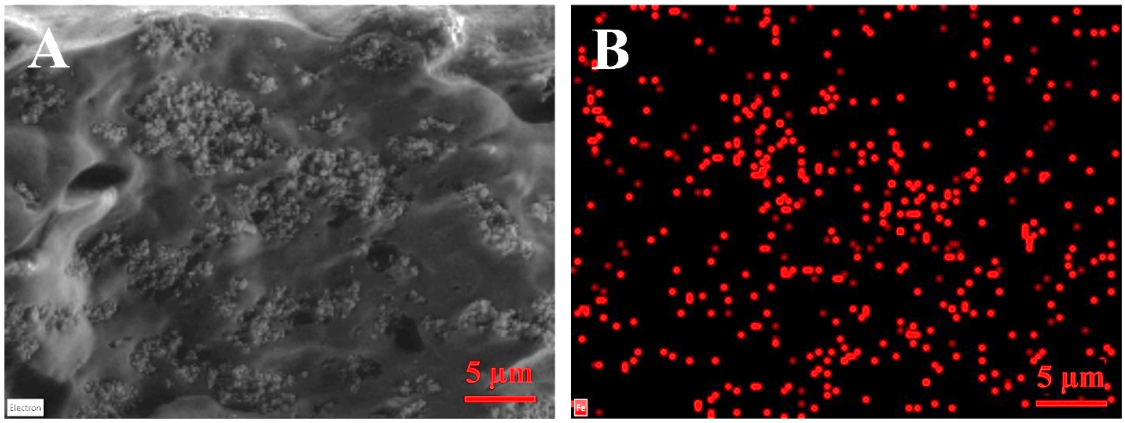

Figure 3. 1: A) SEM images of PHB-INP30 films. **B)** EDS analysis of iron presented in the matrix

Biodegradation

The biodegradation of the nanocomposite films containing 30% w/v INP were assessed through conventional soil burial method previously described.[9] Films square geometry (5×5 cm) were put in an airtight 500 mL chamber containing 200 g of soil (30% humidity). Next, films were buried under an additional 200 g of soil and a gentle pressing was applied to the top layer. Samples were taken out, carefully washed, dried, and weighed after designated time frames. Weight losses were directly attributed to biodegradation. Experiments were performed in triplicates and the time laps were depicted in **Fig. 3.2.**

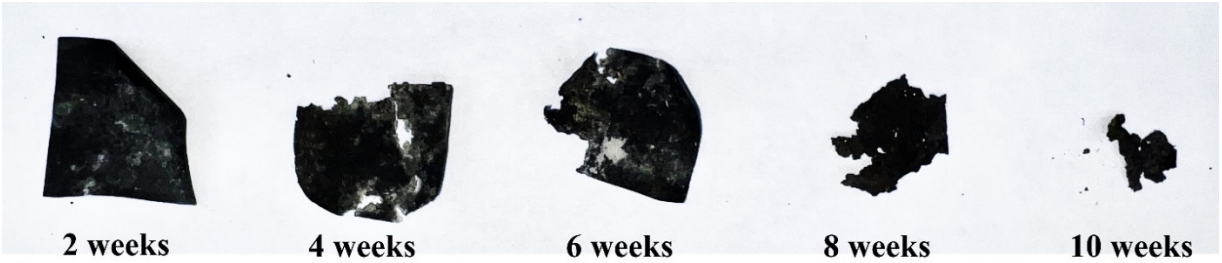

Figure 3. 2: Changes in appearance and size of the films during 10 weeks of soil microbial degradation

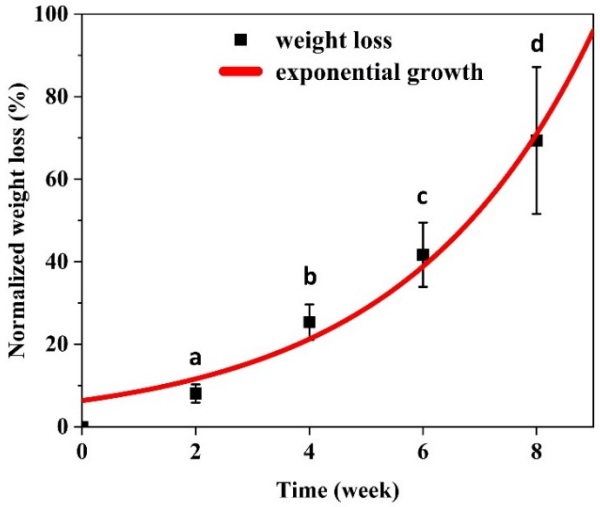

Figure 3. 3: Normalized weight loss of the nanocomposite films during soil microbial degradation. The red line indicates the curved exponential fit. Error bars represent the standard deviation of the mean. Small letters indicate significant difference (one-way ANOVA; $p<0.05$)

These measurements demonstrate a relatively slow degradation rate of the composites within the first 8 weeks from introduction to the soil. The extent of degradation over time was fitted to an exponential curve depicted in **Fig. 3.3** (R^2= 0.965) as explained in **Eq (1)**.

$$weight\ loss\ (\%) = a(1+r)^t \qquad \textbf{Eq. 1}$$

Were a is the constant and equal to 6.37 week^{-1} and r is the degradation rate and equal to 0.35. Exponential increase in weight is an indication of an increase in microorganisms' growth as they consume the substrate as a feed stock.

The release of micronutrients from the NF is believed to be the result of both diffusion through the matrix and erosion.[9] The degradation rate of ~40% and ~70% after 4 and 8 weeks, respectively, demonstrates a controlled release of micronutrients to the soil and crops in within 3 months of soil amendment, which is optimum for maize to fully grow and become ready to harvest (90 days).

POT EXPERIMENTS

130 mm trapezoidal pots (Cord Products, Toronto, Canada) with a height of 100 mm, top diameter of 120 mm and bottom diameter of 100 mm were filled with Soil (400 g dry). In each pot, 3 Maize seeds were planted (5 mm deep). An additional 100 g of soil amended with 0.5% w/w NF powder (0.3 mg INP per kg of soil) covered the planted seeds followed by watering the pots. Two control groups were also studies. The positive control group in which the covering layer of soil is amended with equal amount of naked INP, and negative control group in which the soil was used as is.

Plants were incubated inside a Conviron plant growth chamber (Winnipeg, Canada) equipped with Argus controllers at 40% humidity. The growth chamber simulated cyclic 16 h of daylight at 28 and 22°C followed by 8 h of nighttime at 22°C for 6 weeks. Plants were watered as needed.

After 5 days, two additional germinated seeds were removed from the pot leaving only one growing. Plants were removed from the pot after designated time frames. Plants were cultivated after 16, 21, 26, 31, and 36 days. Plant shoots were detached from the root, and they were washed, air dried, and fully dried to measure the shoot length, dry and wet weight. To dry plants, samples were left in low vacuum oven at 80°C for 48 h. Each experiment was replicated 3 times. The time laps of these experiments are depicted in **Fig. 3.4.**

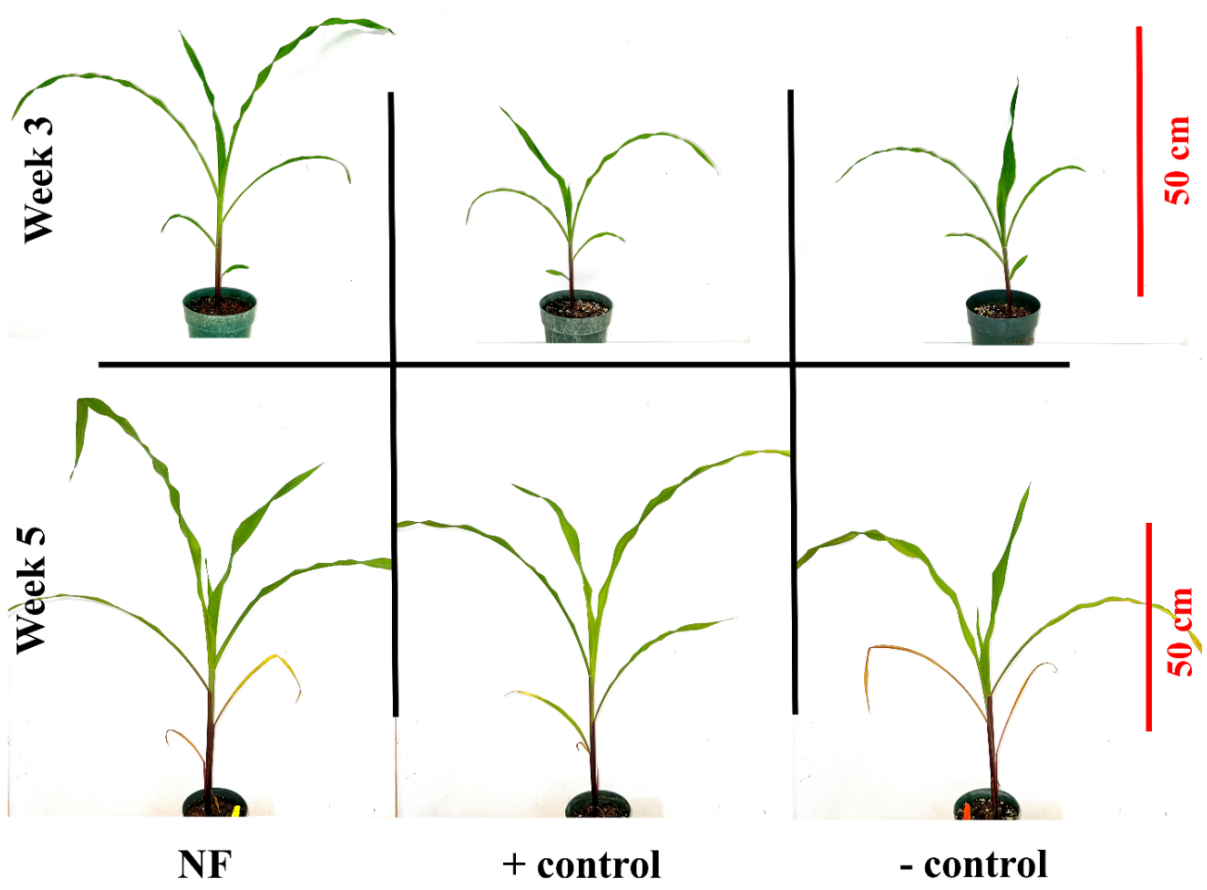

Figure 3. 4: Digital images of Maize grown on soil amended with NF and control groups after 3 weeks (top) and 5 weeks (bottom).

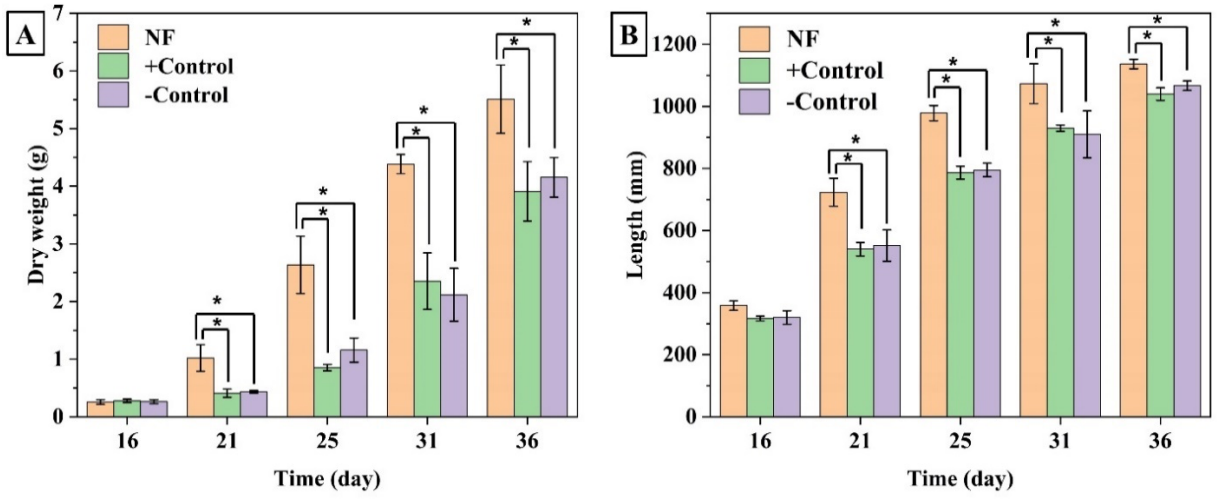

Figure 3. 5: A) Maize dry weight, and **B)** shoot length throughout growing for 36 days. Error bars represent the standard deviation of the mean. Statistical significance of the data (*p < 0.05) was assessed by one-way ANOVA Tukey's test.

The dry weight and shoot length measurement of Maize on and after 21st day of planting demonstrates that the plants grown on soil amended with NF grew faster than both control groups (more mass and length). Until the 16th day of planting, no significant difference was observed in growth of Maize between groups, which could be attributed to the fact that the plant is primarily fed on nutrients provided by the seeds during germination and emergence stage. The results for positive and negative controls were found not significantly different from one another at any time frame indicating that the plants are unable to uptake or metabolize naked INP, possibly due to their high aspect ratio and thus, fast oxidation of Fe^{2+} to Fe^{3+}. As a result, it could be concluded that protecting INP with PHB and its slow release to the soil helps the micronutrient become more bioavailable avoiding consumption by other microorganisms or oxidation to Fe^{3+}.

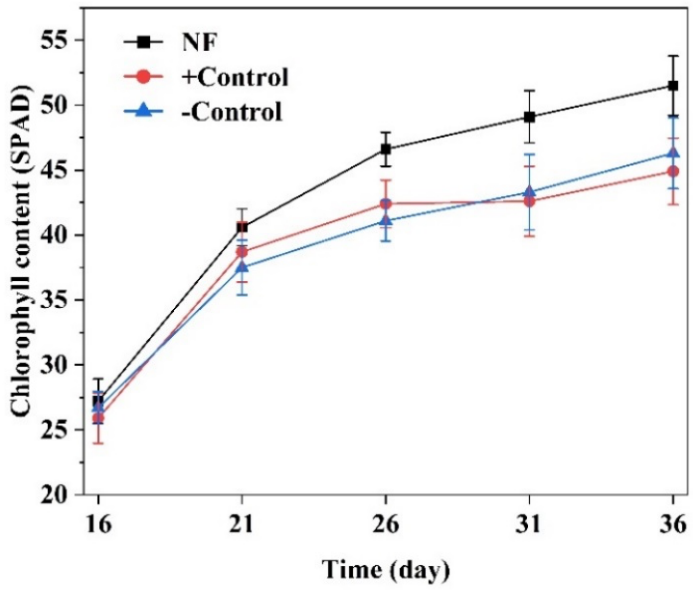

Figure 3. 6: Chlorophyll content of Maize leaves grown on soil amended with NF and control groups.

If faster growth of Maize in NF group is due to the effective delivery of Fe^{2+} micronutrient, a higher chlorophyll content in this group is expected. The reason for this

hypothesis is that Fe^{2+} is crucial micronutrient in several metabolic pathways in plants, including chlorophyll synthesis[10]. Thus, prior to harvesting the plants, chlorophyll content on the leaves was measured using a portable atLEAF CHL Blue chlorophyll meter. For ease of comparison, atLEAF measurements were corrected for Maize to Soil Plant Analysis Development (SPAD) dimensionless units according to a previous report.[11]

CONCLUSION

Here in, we prepared, characterized, and analyzed the effectiveness of a fully biodegradable control release platform for delivery of micronutrients to plants and crops. *E.coli* JM109 was genetically engineered to yield high molecular weight PHB with 65% crystallinity. This high crystallinity of the yielded polymer enabled us to use it for the abovementioned purpose, since it can contain large loads of cargo without completely losing its microcrystalline structure, which is crucial for a degradation-triggered control release system. PHB was loaded with 30% iron nano particles as the micronutrient to prepare the nano fertilizer. Thermal analysis of PHB loaded with 30% w/w cargo demonstrated that the matrix possesses about half of the initial degree of crystallinity, which is a suitable candidate for full degradation in soil within a few months, confirmed by degradation analysis. To assess the effectiveness of prepared nano fertilizer, pot experiments were performed using Maize as the model plant and in a controlled environment. Pot experiments demonstrated that the plants grown on the soil amended with only 0.5% of nano fertilizer on the top layer grow faster, and possess greener leaves, compared with control groups.

Supporting information

Plasmid map and sequence

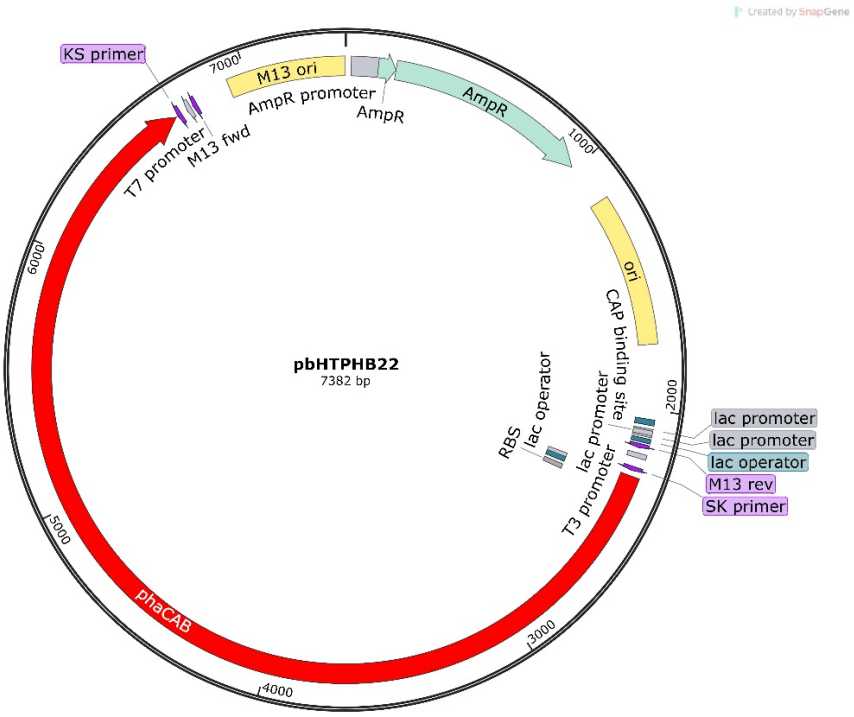

Figure S3. 1: Plasmid map of pbHTPBH22.

Full plasmid pbHTPBH22 sequence is as following:

```
001 GTGGCACTTT TCGGGGAAAT GTGCGCGGAA CCCCTATTTG TTTATTTTTC TAAATACATT
 061 CAAATATGTA TCCGCTCATG AGACAATAAC CCTGATAAAT GCTTCAATAA TATTGAAAAA
 121 GGAAGAGTAT GAGTATTCAA CATTTCCGTG TCGCCCTTAT TCCCTTTTTT GCGGCATTTT
 181 GCCTTCCTGT TTTTGCTCAC CCAGAAACGC TGGTGAAAGT AAAAGATGCT GAAGATCAGT
 241 TGGGTGCACG AGTGGGTTAC ATCGAACTGG ATCTCAACAG CGGTAAGATC CTTGAGAGTT
 301 TTCGCCCCGA AGAACGTTTT CCAATGATGA GCACTTTTAA AGTTCTGCTA TGTGGCGCGG
 361 TATTATCCCG TATTGACGCC GGGCAAGAGC AACTCGGTCG CCGCATACAC TATTCTCAGA
 421 ATGACTTGGT TGAGTACTCA CCAGTCACAG AAAAGCATCT TACGGATGGC ATGACAGTAA
 481 GAGAATTATG CAGTGCTGCC ATAACCATGA GTGATAACAC TGCGGCCAAC TTACTTCTGA
 541 CAACGATCGG AGGACCGAAG GAGCTAACCG CTTTTTTGCA CAACATGGGG GATCATGTAA
 601 CTCGCCTTGA TCGTTGGGAA CCGGAGCTGA ATGAAGCCAT ACCAAACGAC GAGCGTGACA
 661 CCACGATGCC TGTAGCAATG GCAACAACGT TGCGCAAACT ATTAACTGGC GAACTACTTA
 721 CTCTAGCTTC CCGGCAACAA TTAATAGACT GGATGGAGGC GGATAAAGTT GCAGGACCAC
 781 TTCTGCGCTC GGCCCTTCCG GCTGGCTGGT TTATTGCTGA TAAATCTGGA GCCGGTGAGC
 841 GTGGGTCTCG CGGTATCATT GCAGCACTGG GGCCAGATGG TAAGCCCTCC CGTATCGTAG
 901 TTATCTACAC GACGGGGAGT CAGGCAACTA TGGATGAACG AAATAGACAG ATCGCTGAGA
 961 TAGGTGCCTC ACTGATTAAG CATTGGTAAC TGTCAGACCA AGTTTACTCA TATATACTTT
1021 AGATTGATTT AAAACTTCAT TTTTAATTTA AAAGGATCTA GGTGAAGATC CTTTTTGATA
1081 ATCTCATGAC CAAAATCCCT TAACGTGAGT TTTCGTTCCA CTGAGCGTCA GACCCCGTAG
```

1141 AAAAGATCAA AGGATCTTCT TGAGATCCTT TTTTTCTGCG CGTAATCTGC TGCTTGCAAA
1201 CAAAAAAACC ACCGCTACCA GCGGTGGTTT GTTTGCCGGA TCAAGAGCTA CCAACTCTTT
1261 TTCCGAAGGT AACTGGCTTC AGCAGAGCGC AGATACCAAA TACTGTCCTT CTAGTGTAGC
1321 CGTAGTTAGG CCACCACTTC AAGAACTCTG TAGCACCGCC TACATACCTC GCTCTGCTAA
1381 TCCTGTTACC AGTGGCTGCT GCCAGTGGCG ATAAGTCGTG TCTTACCGGG TTGGACTCAA
1441 GACGATAGTT ACCGGATAAG GCGCAGCGGT CGGGCTGAAC GGGGGGTTCG TGCACACAGC
1501 CCAGCTTGGA GCGAACGACC TACACCGAAC TGAGATACCT ACAGCGTGAG CTATGAGAAA
1561 GCGCCACGCT TCCCGAAGGG AGAAAGGCGG ACAGGTATCC GGTAAGCGGC AGGGTCGGAA
1621 CAGGAGAGCG CACGAGGGAG CTTCCAGGGG GAAACGCCTG GTATCTTTAT AGTCCTGTCG
1681 GGTTTCGCCA CCTCTGACTT GAGCGTCGAT TTTTGTGATG CTCGTCAGGG GGGCGGAGCC
1741 TATGGAAAAA CGCCAGCAAC GCGGCCTTTT TACGGTTCCT GGCCTTTTGC TGGCCTTTTG
1801 CTCACATGTT CTTTCCTGCG TTATCCCCTG ATTCTGTGGA TAACCGTATT ACCGCCTTTG
1861 AGTGAGCTGA TACCGCTCGC CGCAGCCGAA CGACCGAGCG CAGCGAGTCA GTGAGCGAGG
1921 AAGCGGAAGA GCGCCCAATA CGCAAACCGC CTCTCCCCGC GCGTTGGCCG ATTCATTAAT
1981 GCAGCTGGCA CGACAGGTTT CCCGACTGGA AAGCGGGCAG TGAGCGCAAC GCAATTAATG
2041 TGAGTTAGCT CACTCATTAG GCACCCCAGG CTTTACACTT TATGCTTCCG GCTCGTATGT
2101 TGTGTGGAAT TGTGAGCGGA TAACAATTTC ACACAGGAAA CAGCTATGAC CATGATTACG
2161 CCAAGCGCGC AATTAACCCT CACTAAAGGG AACAAAAGCT GGAGCTCCAC CGCGGTGGCG
2221 GCCGCTCTAG AACTAGTGGA TCCCCCGGGC TGCAGGAATT CGATAATTAA TACGACTCAC
2281 TATAGGGGAA TTGTGAGCGG ATAACAATTC CCCTCTAGAA ATAATTTTGT TTAACTTTAA
2341 GAAGGAGATA TACATATGGC CACCGGTAAA GGCGCAGCAG CCAGTACCCA GGAAGGTAAA
2401 AGTCAGCCGT TTAAAGTTAC CCCGGGTCCG TTTGATCCGG CAACCTGGCT GGAATGGAGC
2461 CGTCAGTGGC AGGGCACCGA AGGCAATGGT CATGCAGCAG CCAGCGGCAT TCCGGGTCTG
2521 GATGCACTGG CCGGTGTTAA AATTGCCCCG GCACAGCTGG GCGATATTCA GCAGCGTTAT
2581 ATGAAAGATT TTAGTGCACT GTGGCAGGCA ATGGCCGAAG GCAAAGCCGA AGCCACCGGT
2641 CCGCTGCATG ATCGCCGCTT TGCAGGTGAC GCCTGGCGCA CCAATCTGCC GTATCGCTTT
2701 GCAGCCGCAT TTTATCTGCT GAATGCACGC GCCCTGACCG AACTGGCAGA TGCAGTGGAA
2761 GCAGATGCCA AAACCCGCCA GCGCATTCGT TTTGCAATTA GCCAGTGGGT GGATGCAATG
2821 AGTCCGGCAA ATTTTCTGGC CACCAATCCG GAAGCCCAGC GCCTGCTGAT TGAAAGCGGC
2881 GGCGAAAGTC TGCGCGCAGG TGTTCGTAAT ATGATGGAAG ATCTGACCCG TGGTAAAATT
2941 AGCCAGACCG ATGAAAGTGC ATTTGAAGTG GGCCGTAATG TTGCCGTTAC CGAAGGTGCC
3001 GTTGTGTTTG AAAATGAATA TTTTCAGCTG CTGCAGTATA AACCGCTGAC CGATAAAGTT
3061 CATGCACGCC CGCTGCTGAT GGTGCCGCCG TGTATTAATA AGTATTATAT TCTGGACCTG
3121 CAGCCGGAAA GTAGTCTGGT GCGTCATGTT GTTGAACAGG GTCATACCGT TTTTCTGGTT
3181 AGCTGGCGCA ATCCGGATGC CAGCATGGCC GGCAGCACCT GGGATGATTA TATTGAACAT
3241 GCAGCAATTC GTGCCATTGA AGTTGCCCGC GATATTAGTG GTCAGGATAA AATTAATGTG
3301 CTGGGCTTTT GTGTGGGCGG CACCATTGTG AGCACCGCCC TGGCCGTTCT GGCCGCTCGT
3361 GGTGAACATC CGGCCGCCAG CGTTACCCTG CTGACCACCC TGCTGGATTT TGCCGATACC
3421 GGCATTCTGG ATGTGTTTGT GGATGAAGGT CATGTTCAGC TGCGTGAAGC CACCCTGGGT
3481 GGCGGTGCCG GTGCACCTTG TGCACTGCTG CGCGGCCTGG AACTGGCAAA TACCTTTAGC
3541 TTTCTGCGCC CGAATGATCT GGTGTGGAAT TATGTGGTGG ATAATTATCT GAAAGGCAAT
3601 ACCCCGGTGC CGTTTGATCT GCTGTTTTGG AATGGCGATG CAACCAATCT GCCTGGTCCG
3661 TGGTATTGTT GGTATCTGCG TCATACCTAT CTGCAGAATG AACTGAAAGT TCCGGGTAAA
3721 CTGACCGTTT GCGGTGTTCC GGTTGATCTG GCAAGTATTG ATGTGCCGAC CTATATCTAT
3781 GGCAGTCGCG AAGATCATAT TGTGCCGTGG ACCGCCGCAT ATGCAAGTAC CGCACTGCTG
3841 GCCAATAAGC TGCGCTTTGT TCTGGGCGCC AGTGGTCATA TTGCCGGTGT TATTAATCCG
3901 CCGGCAAAAA ATAAGCGTAG CCATTGGACC AATGATGCCC TGCCGGAAAG CCCGCAGCAG
3961 TGGCTGGCCG GTGCCATTGA ACATCATGGC AGCTGGTGGC CGGATTGGAC CGCCTGGCTG
4021 GCCGGACAGG CAGGTGCTAA ACGCGCAGCA CCGGCAAATT ATGGTAATGC CCGTTATCGT
4081 GCAATTGAAC CGGCACCGGG TCGTTATGTT AAAGCAAAAG CCGTGCTGGC CGTGATTGAT
4141 AAACGCGGTG GTGGCGGCGG TAGTGGCGGT GGTAGTGGTG GTGGTAGTGG CGGCGGCGGC
4201 AGCATGCCTG CAGCAGTTCC GGGCCTGTGT GGCCTGCGCC GTGGTACAAG TCCGCATATG
4261 GTGCCGGCAG TGCCGGGCAC CCTGGTGTGG ACACCGAGCG CAGTTCAGAA AATTAAGGAA
4321 CTGCTGAAAG ATAAACCGGA ACATGTGGGT GTTAAAGTGG GTGTGCGTAC CCGCGGCTGC
4381 AATGGTCTGA GTTATACCCT GGAATATACC AAAAGTAAAG GTGACAGCGA TGAAGAAGTT
4441 GTTCAGGATG GCGTTCGCGT GTTTATTGAA AAGAAAGCCC AGCTGACCCT GCTGGGTACC
4501 GAAATGGATT ATGTTGAAGA TAAACTGAGT AGCGAATTTG TTTTTAACAA CCCGAATATT

4561 AAGGGCACCT GTGGTTGTGG CGAAAGCTTT AATATTTAAC GCTTGCATGA GTGCCGGCGT
4621 GCGTCATGCA CGGCGCCGGC AGGCCTGCAC GTTCCCTCCC GTTTCCATTG AAAGGACTAC
4681 ACAATGACCG ATGTGGTTAT TGTGAGTGCA GCACGTACCG CAGTGGGCAA ATTTGGTGGT
4741 AGCCTGGCCA AAATTCCGGC CCCGGAACTG GGCGCAGTGG TTATTAAGGC AGCCCTGGAA
4801 CGCGCCGGTG TGAAACCGGA ACAGGTTAGC GAAGTTATTA TGGGTCAGGT GCTGACCGCC
4861 GGTAGCGGTC AGAATCCGGC ACGCCAGGCA GCAATTAAGG CAGGTCTGCC GGCCATGGTT
4921 CCGGCCATGA CCATTAATAA GGTTTGCGGC AGTGGCCTGA AAGCCGTTAT GCTGGCCGCA
4981 AATGCAATTA TGGCAGGTGA CGCCGAAATT GTGGTGGCCG GCGGCCAGGA AAATATGAGT
5041 GCCGCCCCGC ATGTGCTGCC GGGCAGTAGA GATGGTTTTC GCATGGGCGA TGCCAAACTG
5101 GTGGATACCA TGATTGTTGA TGGTCTGTGG GATGTGTATA ATCAGTATCA TATGGGTATT
5161 ACCGCCGAAA ATGTTGCAAA AGAATATGGT ATTACCCGCG AAGCCCAGGA TGAATTTGCA
5221 GTGGGCAGCC AGAATAAGGC CGAAGCCGCA CAGAAAGCCG GCATGTTTGA TGAAGAAATT
5281 GTTCCGGTTC TGATTCCGCA GCGTAAAGGC GATCCGGTTG CATTCAAAAC CGATGAATTT
5341 GTGCGTCAGG GCGCCACCCT GGATAGCATG AGCGGTCTGA AACCGGCCTT TGATAAAGCC
5401 GGTACCGTGA CCGCCGCAAA TGCGAGCGGT CTGAATGATG GCGCAGCCGC AGTGGTTGTT
5461 ATGAGCGCAG CCAAAGCCAA AGAACTGGGT CTGACCCCGC TGGCAACCAT TAAGAGCTAT
5521 GCCAATGCAG GTGTGGATCC GAAAGTGATG GGCATGGGCC CGGTGCCGGC CAGTAAACGT
5581 GCACTGAGCC GCGCCGAATG GACCCCGCAG GATCTGGATC TGATGGAAAT TAATGAAGCC
5641 TTTGCAGCAC AGGCACTGGC AGTTCATCAG CAGATGGGCT GGGATACCAG TAAAGTTAAT
5701 GTTAATGGTG GTGCCATTGC AATTGGCCAT CCGATTGGTG CAAGCGGTTG CCGTATTCTG
5761 GTTACCCTGC TGCATGAAAT GAAACGCCGC GATGCCAAAA AAGGTCTGGC CAGCCTGTGC
5821 ATTGGTGGTG GTATGGGTGT TGCACTGGCC GTTGAACGTA AATAAGGAAG GGGTTTTCCG
5881 GGGCCGCGCG CGGTTGGCGC GGACCCGGCG ACGATAACGA AGCCAATCAA GGAGTGGACA
5941 TGACCCAGCG TATTGCCTAT GTGACCGGCG GTATGGGTGG TATTGGTACC GCCATTTGTC
6001 AGCGCCTGGC AAAAGATGGC TTTCGTGTGG TTGCAGGTTG TGGTCCGAAT AGTCCGCGTC
6061 GTGAAAAATG GCTGGAACAG CAGAAAGCCC TGGGTTTTGA TTTTATTGCC AGCGAAGGCA
6121 ATGTGGCAGA TTGGGATAGT ACCAAAACCG CATTTGATAA AGTTAAAAGT GAGGTGGGCG
6181 AAGTTGATGT GCTGATTAAT AATGCCGGTA TTACCCGCGA TGTTGTGTTT CGTAAAATGA
6241 CCCGCGCCGA TTGGGATGCA GTGATTGATA CCAATCTGAC CAGTCTGTTT AATGTTACCA
6301 AACAGGTTAT TGATGGTATG GCCGATCGTG GCTGGGGTCG CATTGTTAAT ATTAGTAGCG
6361 TTAATGGTCA GAAAGGTCAG TTTGGCCAGA CCAATTATAG CACCGCAAAA GCAGGTCTGC
6421 ATGGTTTTAC CATGGCCCTG GCCCAGGAAG TTGCCACCAA AGGTGTTACC GTGAATACCG
6481 TTAGCCCGGG CTATATTGCC ACCGATATGG TTAAAGCAAT TCGCCAGGAT GTTCTGGATA
6541 AAATTGTGGC CACCATTCCG GTGAAACGTC TGGGCCTGCC GGAAGAAATT GCCAGTATTT
6601 GCGCATGGCT GAGTAGCGAA GAAAGCGGCT TTAGTACCGG CGCCGATTTT AGCCTGAATG
6661 GTGGCCTGCA TATGGGCTAA CCTGCATCAA GCTTATCGAT ACCGTCGACC TCGAGGGGGG
6721 GCCCGGTACC CAATTCGCCC TATAGTGAGT CGTATTACGC GCGCTCACTG GCCGTCGTTT
6781 TACAACGTCG TGACTGGGAA AACCCTGGCG TTACCCAACT TAATCGCCTT GCAGCACATC
6841 CCCCTTTCGC CAGCTGGCGT AATAGCGAAG AGGCCCGCAC CGATCGCCCT TCCCAACAGT
6901 TGCGCAGCCT GAATGGCGAA TGGGACGCGC CCTGTAGCGG CGCATTAAGC GCGGCGGGTG
6961 TGGTGGTTAC GCGCAGCGTG ACCGCTACAC TTGCCAGCGC CCTAGCGCCC GCTCCTTTCG
7021 CTTTCTTCCC TTCCTTTCTC GCCACGTTCG CCGGCTTTCC CCGTCAAGCT CTAAATCGGG
7081 GGCTCCCTTT AGGGTTCCGA TTTAGTGCTT TACGGCACCT CGACCCCAAA AAACTTGATT
7141 AGGGTGATGG TTCACGTAGT GGGCCATCGC CCTGATAGAC GGTTTTTCGC CCTTTGACGT
7201 TGGAGTCCAC GTTCTTTAAT AGTGGACTCT TGTTCCAAAC TGGAACAACA CTCAACCCTA
7261 TCTCGGTCTA TTCTTTTGAT TTATAAGGGA TTTTGCCGAT TTCGGCCTAT TGGTTAAAAA
7321 ATGAGCTGAT TTAACAAAAA TTTAACGCGA ATTTTAACAA AATATTAACG CTTACAATTT
7381 AG

Pot experiments

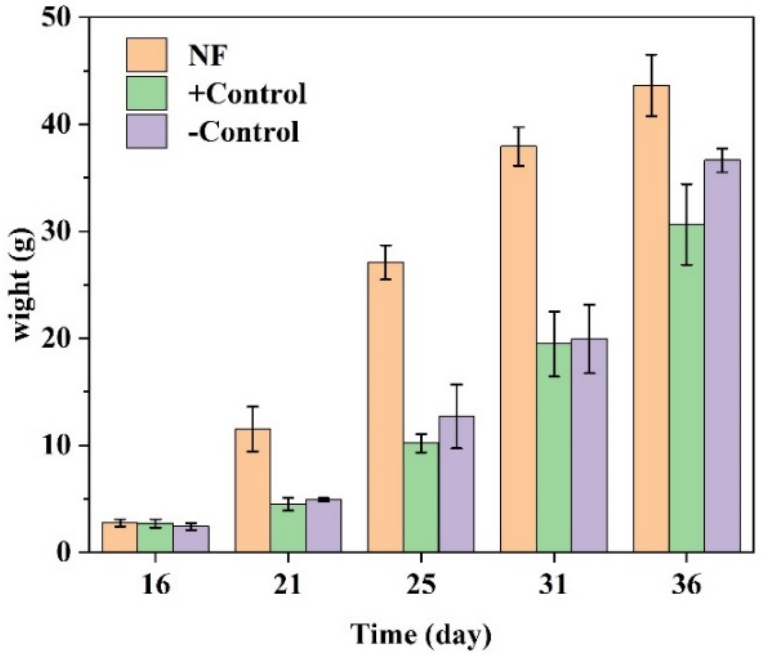

Figure S3. 2: Maize shoot weight throughout growing for 36 days.

Soil analysis

Soil pH, Organic Matter, extractable P, K, Mg, Fe, Mn, Al, Ca, Cu, S, B, organic and total carbon, and total nitrogen were measured Cornell Soil Health Labs. Information regarding the protocols used could be found at their website https://soilhealthlab.cals.cornell.edu/

References

(1) Guha, T.; Gopal, G.; Kundu, R.; Mukherjee, A. Nanocomposites for Delivering Agrochemicals: A Comprehensive Review. *Journal of Agricultural and Food Chemistry* **2020**, *68* (12), 3691–3702.

(2) Torabi, H.; Mosleh, I.; Davachi, S. M.; Davaritouchaee, M.; Abbaspourrad, A. Xylose-Rich Horse Manure Hydrolysate as the Sole Carbon Source for Bacterial Production of Polyhydroxy Butyrate Using Engineered Escherichia Coli. *ACS Sustainable Chemistry & Engineering* **2021**, *9* (27), 8946–8950.

(3) Davachi, S. M.; Kaffashi, B.; Torabinejad, B.; Zamanian, A.; Seyfi, J.; Hejazi, I. Investigating Thermal, Mechanical and Rheological Properties of Novel Antibacterial Hybrid Nanocomposites Based on PLLA/Triclosan/Nano-Hydroxyapatite. *Polymer* **2016**, *90*, 232–241.

(4) Davoodi, S.; Oliaei, E.; Davachi, S. M.; Hejazi, I.; Seyfi, J.; Heidari, B. S.; Ebrahimi, H. Preparation and Characterization of Interface-Modified PLA/Starch/PCL Ternary Blends Using PLLA/Triclosan Antibacterial Nanoparticles for Medical Applications. *RSC Advances* **2016**, *6* (46), 39870–39882.

(5) Sahraeian, R.; Davachi, S. M.; Heidari, B. S. The Effect of Nanoperlite and Its Silane Treatment on Thermal Properties and Degradation of Polypropylene/Nanoperlite Nanocomposite Films. *Composites Part B: Engineering* **2019**, *162*, 103–111. https://doi.org/10.1016/j.compositesb.2018.10.093.

(6) Modi, S.; Koelling, K.; Vodovotz, Y. Assessment of PHB with Varying Hydroxyvalerate Content for Potential Packaging Applications. *European Polymer Journal* **2011**, *47* (2), 179–186. https://doi.org/10.1016/j.eurpolymj.2010.11.010.

(7) Kusaka, S.; Iwata, T.; Doi†*, Y. Microbial Synthesis and Physical Properties of Ultra-High-Molecular-Weight Poly [(R)-3-Hydroxybutyrate]. *Journal of Macromolecular Science, Part A: Pure and Applied Chemistry* **1998**, *35* (2), 319–335.

(8) Fan, K. W.; Chen, F. Bioprocessing for Value-Added Products from Renewable Resources. *Shang, TY Elsevier Science* **2007**, *684*.

(9) Daitx, T. da S.; de Lima, V. S.; Gryczak, M.; Petzhold, C. L.; Carli, L. N.; Mauler, R. S. Poly (Hydroxybutyrate)-based Systems Behavior on the Controlled Release of NPK Fertilizers. *Polymers for Advanced Technologies* **2020**, *31* (11), 2579–2587.

(10) Wang, M.; Zhang, G.; Zhou, L.; Wang, D.; Zhong, N.; Cai, D.; Wu, Z. Fabrication of PH-Controlled-Release Ferrous Foliar Fertilizer with High Adhesion Capacity Based on Nanobiomaterial. *ACS Sustainable Chemistry & Engineering* **2016**, *4* (12), 6800–6808.

(11) Zhu, J.; Tremblay, N.; Liang, Y. Comparing SPAD and AtLEAF Values for Chlorophyll Assessment in Crop Species. *Canadian journal of soil science* **2012**, *92* (4), 645–648.

Chapter 4: Conclusion and Future Approaches

Today, it is estimated that over 12 million tons of plastic wastes enter the oceans annually, posing a serious danger to the marine ecosystem and subsequently, food chain. Thus, to mitigate issues posed by such materials, replacing petroleum-based plastics with biodegradable ones is inevitable since attempts to recycling or chemical and thermal degradation of non-biodegradable plastics were not found completely successful.

PHA is a family of polyesters which can effectively replace non-biodegradable plastics, due to their satisfactory physiochemical properties. However, large scale production of such materials is limited due to the high cost of production. Several research groups have made great progress in chemical synthesis of a variety of PHAs in terms of catalyst designs and monomer synthesis. However, the production costs using synthetic routes are orders of magnitude greater than microbial production. On the other hand, microbial production has its own limitations, most importantly, costs associated with carbon source, or feed stock. In this regard, we proved the waste-to-value concept of processability and use of manure as the sole carbon source for microbial production of PHA. Currently, large scale producers of PHA were able to reduce the price of their products to 2-5 USD per kg. However, it is still not comparable to that of poly olefins (e.g., polyethylene) which are less than one USD per kg. We believe this waste-to-value approach not only has the potential to reduce the production costs, but also addresses the general concerns associated with management several types of wastes. A wide variety of agricultural and food wastes can be used for this purpose and full discovery of their potential for this application requires immense research and development.

PHA are also studied for a variety of applications especially, in biomedical sciences. Non-toxicity and full biodegradability of PHA has made them a great candidate for drug and nucleic acid delivery, tissue engineering, packaging, wound healing, and oral drugs. In

agricultural industry, the application of PHA is studied for mulch films, agricultural nets, and grow bags. Interestingly, very few studies have been reported regarding the direct use of PHA as fertilizer coatings or nano fertilizer. High crystallinity and biodegradability of PHA gives it a great undiscovered potential for approaching a controlled release system to deliver traditional and modern nutrients to the soil, plants, and crops. In addition to that, microplastics of PHA can be used for fragrance and flavor encapsulations in detergents and even food industry since a few of PHA family members have already received FDA approval for oral consumption.

Research and development of biodegradable plastics, including PHA, and their incorporation into the modern world products requires biodegradation studies. The current standard test methods are not only time taking, but also hard to reproduce the results. Thus, the need for a rapid, high throughput, standardized test method yielding highly repeatable and reproducible results is felt among scholars and scientists. Thus, we developed a microfluidic system which provides time-resolved data for enzymatic degradation of polymer microparticles. Using microfluidic technique, we were able to replace the secondary, and somewhat sophisticated, costly, and time taking analytical test methods by image processing techniques.

To advance this method and accurately elucidate the kinetics of degradation, a mathematical model was developed and validated by the integration of chemical mechanisms and the associated transport phenomena (heat, mass, and momentum transfer). Previously reported kinetic models for such reactions were only taking proposed chemical reactions into account. Microfluidic system allowed us to minimize the effect of momentum transfer, which resembles natural microbial degradation more than other previously reported rapid methods. On the other hand, the effect of heat transfer in this environment is not well understood as all the experiments were performed at isothermal conditions (room temperature). The effect of

temperature, pH, salinity, and synergy of a group of enzymes on degradation kinetics could be studied using the developed microfluidic technique and further modify our proposed SPM-SCM kinetic models, accordingly. Incorporating artificial intelligence for image processing and mechanized microscopy can drastically decrease the time required for read outs by automation of the tests yielding to more accurate and rapid results.